

**RESEARCH AND DESIGN OF THREE-PHASE HIGH FREQUENCY RECTIFIER
WITH VOLTAGE BOOSTING AND POWER FACTOR CORRECTION
CAPABILITY**

ManZhiyao

**A project report submitted in partial fulfilment of the
requirements for the award of Master of Engineering (Electrical)**

**Lee Kong Chian Faculty of Engineering and Science
Universiti Tunku Abdul Rahman**

April 2024

DECLARATION

I hereby declare that this project report is based on my original work except for citations and quotations which have been duly acknowledged. I also declare that it has not been previously and concurrently submitted for any other degree or award at UTAR or other institutions.

Signature : Man, Zhiyao

Name : Man, Zhiyao

ID No. : 2200004

Date : 4 April 2024

APPROVAL FOR SUBMISSION

I certify that this project report entitled “**Research and Design of Three-phase High frequency rectifier with voltage boosting and power factor correction capability**” was prepared by **Man,Zhiyao** has met the required standard for submission in partial fulfilment of the requirements for the award of Master of Engineering (Electrical) at Universiti Tunku Abdul Rahman.

Approved by,

Signature : 

Supervisor : Dr.Chew Kuew Wai

Date : 4 April 2024

Signature : _____

Co-Supervisor : None

Date : None

The copyright of this report belongs to the author under the terms of the copyright Act 1987 as qualified by Intellectual Property Policy of Universiti Tunku Abdul Rahman. Due acknowledgement shall always be made of the use of any material contained in, or derived from, this report.

© 2024, Man,Zhiyao All right reserved.

ACKNOWLEDGEMENTS

I would like to thank everyone who had contributed to the successful completion of this project. I would like to express my gratitude to my research supervisor, Dr. Chew Kuew Wai for his invaluable advice, guidance and his enormous patience throughout the development of the research.

ABSTRACT

With the popularization of various power electronic devices, harmonic pollution of power grid becomes more and more serious. Among them, the traditional rectifier is one of the main sources of power grid pollution. As a new generation of rectifier, three-phase voltage PWM rectifier has the characteristics of constant output voltage, unity power factor operation and low harmonic pollution. The purpose of this paper is to develop a three-phase PWM rectifier device. Firstly, the circuit structure and control principle of PWM rectifier are briefly described, and the operation modes of three-phase voltage type PWM rectifier (Voltage Source Rectifier VSR) under different switching modes are analyzed. By switching function and coordinate transformation, to establish the general mathematical model of three-phase VSR and DQ(Cartesian coordinates Real part and Imaginary part) mathematical model. According to the established mathematical model, the design process of voltage and current control loop controller is introduced in detail. Secondly, the Matlab/Simulink simulation platform is used to build the simulation system model. Finally, By comparing the simulation and result analysis, the feasibility of the control scheme in this paper is verified. Based on the above process, a three-phase PWM rectifier with variable output voltage and adjustable grid side power factor was finally implemented, bringing research prospects for harmonic control in the power grid.

TABLE OF CONTENTS

DECLARATION	ii
APPROVAL FOR SUBMISSION	iii
ACKNOWLEDGEMENTS	v
ABSTRACT	vi
TABLE OF CONTENTS	vii
LIST OF TABLES	ix
LIST OF FIGURES	x
LIST OF SYMBOLS / ABBREVIATIONS	xi
LIST OF APPENDICES	xii

CHAPTER

1	INTRODUCTION	1
	1.1 General Introduction	1
	1.2 Importance of the Study	1
	1.3 Aims and Objectives	2
2	LITERATURE REVIEW	4
	2.1 Introduction	4
	2.2 Review Research on PWM rectifier topology and mathematical model	5
	2.3 Research on PWM rectifier control technology	6
	2.4 Summary	11
3	RESEARCH METHODOLOGY	12
	3.1 Introduction	12
	3.2 Mathematical models	15
	3.3 Analysis of Double Closed Loop Linear Control	17

3.3.1	PI current inner loop design	18
3.3.2	PI voltage outer loop design	20
3.4	Design of inductance and capacitor	21
3.4.1	Design of AC side inductance	21
3.4.2	Design of DC side capacitor	23
3.4.3	Selection of Power Electronic Switch	24
3.5	Summary	24
4	RESULTS AND DISCUSSIONS	25
4.1	Introduction	25
4.2	Simulation Model Building	25
4.3	Simulation waveform analysis	28
4.4	Summary	35
5	CONCLUSIONS AND RECOMMENDATIONS	36
5.1	Conclusions	36
5.2	Recommendations for future work	36
	REFERENCES	37
	APPENDICES	39

LIST OF TABLES

Table2.1	Classification Table	5
Table2.2	Control strategies Table	7
Table4.1	Simulation parameters	25

LIST OF FIGURES

Figure 2.1 amplitude and phase control	7
Figure 2.2 direct current regulation	7
Figure 2.3 direct power control	8
Figure 2.4 Variable Structure Control with Sliding Mode	9
Figure 2.5 feedback linearization control	10
Figure 2.6 Lyapunov stability theory control	11
Figure 3.1 Three phase voltage type PWM rectifier circuit	12
Figure 3.2 Model circuit of rectifier	13
Figure 3.3 Steady State Vector Relationship on AC Side of PWM Rectifier	14
Figure 3.4 dq mathematical model	17
Figure 3.5 Structure of feedforward decoupling PI control system	18
Figure 3.6 Current Inner Ring Structure Diagram	18
Figure 3.7 Simplified current inner loop structure diagram	18
Figure 3.8 Voltage outer loop control structure	20
Figure 3.9 Simplified controller structure for voltage outer loop	21
Figure 3.10 Diagram of steady-state vector relationship on the AC side	22
Figure 4.1 Simulation Model	26
Figure 4.2 Decoupling Control	26
Figure 4.3 Phase Locked Loop and Coordinate Transformation	26
Figure 4.4 SVPWM model	28
Figure 4.5 DC Bus Voltage	28
Figure 4.6 Waveform of A-phase Voltage and A-phase Current	29
Figure 4.7 Three phase voltage and circuit waveform diagram	29
Figure 4.8 THD diagram of phase A	30
Figure 4.9 Waveform of DC Bus Voltage	30
Figure 4.10 Waveform of A-phase Voltage and A-phase Current	31
Figure 4.11 Waveform of three-phase voltage and current	31
Figure 4.12 THD analysis diagram of A-phase current	32
Figure 4.13 Simulated circuit diagram	33
Figure 4.14 Voltage and current waveform diagram	34

LIST OF SYMBOLS / ABBREVIATIONS

PWM	Pulse Width Modulation
DC	Direct Current
AC	Alternating Current
e_a	A-phase voltage
e_b	B-phase voltage
e_c	C-phase voltage
i_a	A-phase current
i_b	B-phase current
i_c	C-phase current
L	network side inductance
T	switching
C	DC capacitor
R_L	output resistance
R	inductive internal resistance
v_L	inductance voltage
v_{RL}	output resistance voltage
v_{dc}	DC output voltage
i_{dc}	DC output current
Sk	logic switching function
f	grid frequency
w	Grid angle radian

LIST OF APPENDICES

APPENDIX A : Graphs	39
APPENDIX B : Tables	41

CHAPTER 1

INTRODUCTION

1.1 General Introduction

Among various loads in the power system, time-varying nonlinear loads (such as motors, transformers, etc.) and power electronic converters account for the largest proportion. The widespread application of these loads has greatly improved production efficiency and people's quality of life, while also generating harmonic interference and reactive power on the input grid side, reducing transmission quality.

Harmonics in the power grid can seriously affect industry, agriculture, and people's lives. It reduces power quality and transmission efficiency, causing overheating, vibration and other phenomena in electrical equipment, reducing the stability of electrical equipment, and damaging its related components, greatly reducing its lifespan. For the power system, when harmonics exceed a certain standard limit, the energy storage components in the circuit will generate series or parallel resonance, causing serious damage to capacitors and other devices. At the same time, it will misoperate the relay protection device, greatly reduce the accuracy of the energy metering device, and also affect communication facilities, increasing additional losses. Therefore, in many application places with strict requirements for the performance indicators of the power grid side, the selection of connected inverters is strictly in accordance with international harmonic standards, resulting in a broader development prospect for low harmonic converter devices. Simultaneously, the exploration of harmonics not only constitutes a pivotal aspect within inverter investigations but also stands as a crucial avenue within power electronics technology, fostering advancements in the field.

1.2 Importance of the Study

In response to the hazards of harmonics, the academic community has proposed corresponding methods for harmonic control. There are two conventional ways to control power harmonic pollution: passive compensation and active compensation. However, both passive and active compensation belong to the passive method of post compensation, which compensates for the generated harmonics by adding a filtering

circuit to the inverter device. Starting from another perspective, in response to the fact that the vast majority of harmonics in the power system are generated by the inverter itself, actively transforming the inverter device itself to eliminate the harmonic source, making the input current sinusoidal and eliminating its reactive power component, and achieving unit power factor operation, is the most fundamental measure to control harmonic and reactive power pollution in the power grid.

PWM rectification adopts fully controlled devices, transplanting the mature pulse width modulation control technology used in the inverter circuit. Through a well-designed control algorithm, the fully controlled switching devices are finely controlled to achieve the expected goals. Compared with power factor correction(PFC) technology, the input current waveform is more sinusoidal, the dynamic response is faster, energy can flow in both directions, and the power factor is switched between positive and negative values, improving the power quality from the root and achieving green transformation. Therefore, the research on PWM rectification technology is of great practical significance for achieving a resource-saving society and the development of the energy field.

However, the control algorithm is the core of the PWM rectifier. Due to the fact that PWM rectifiers are nonlinear systems, there are problems such as slow dynamic response, strong dependence on system parameters, and reduced effectiveness in controlling uncertain disturbances when using linear system control; In control theory, nonlinear system control can accelerate the dynamic response of the system, weaken the dependence on system parameters, and enhance the robustness to external disturbances, resulting in better control effects. Therefore, studying the use of nonlinear control methods in PWM rectification is of great significance for improving the control effect of inverters, reducing input grid side harmonics, solving reactive power pollution, and improving power quality and utilization.

1.3 Aims and Objectives

Given its straightforward circuit design, superior control capabilities, and capacity to function across four quadrants, the three-phase voltage type PWM rectifier operates with a low harmonic footprint while maintaining a unity power factor, aligning with environmental preservation and energy efficiency goals. Consequently, this paper selects the three-phase voltage type pulse width modulation rectifier as its focus and primarily investigates the following areas:

(1) Conduct an in-depth examination of the structure and operational principles of the three-phase voltage-type pulse width modulation rectifier under study. Analyze the current switching process during rectification and inversion phases, and tailor the main circuit parameters in accordance with system specifications.

(2) Develop a comprehensive understanding of the primary circuit layout, establishing mathematical models for the three-phase voltage source rectifier within both the stationary and synchronous rotating coordinate systems. Following this, devise a dual closed-loop control system and investigate voltage space vector modulation techniques.

(3) A simulation model of rectifier under grid balance was designed, and steady-state rectification under grid balance was simulated. The simulation and theoretical results were analyzed and studied.

CHAPTER 2

LITERATURE REVIEW

2.1 Introduction

The research on PWM technology emerged in the 1980s, and due to the widespread application and promotion of fully controlled switching devices that emerged at the same time, it attracted widespread attention in the academic community.

In the early 1980s, scholars Busse Alfred and Holtz Joachim were the first to discover a full bridge topology, and they successfully achieved grid side current sinusoidal transformation. Subsequently, various researchers have made achievements in control strategies, from the conversion of current type to voltage type topology, the leap from continuous to discrete mathematical models of systems, and the rise of PWM rectifiers have aroused the research interest of experts and scholars, becoming a hot topic in the field of power electronics. Topological structures and control methods continue to extend and are applied in various fields of research. The research on related technologies and applications further promotes the development and improvement of their topology and control technologies.

Since the 1990s, there has been a surge of global interest among researchers in the exploration and enhancement of three-phase rectifiers. This period coincided with the introduction of digital processing chips, facilitating the adoption of digital control for PWM rectification and streamlining its application. After entering the 21st century, more novel control strategies have been proposed, and their application scope is gradually expanding. The topology structure and control methods are also more specific. According to the differences in grid side connection methods, it can be divided into single-phase rectifiers, three-phase rectifiers, and multiphase rectifiers. Based on the diverse methods of energy storage on the DC side, classification can be made into voltage-based rectifiers and current-based rectifiers. Additionally, categorization based on distinctions in switching modulation techniques leads to the classification into soft switching modulation and hard switching modulation. In addition, there are many classification methods based on the level. Electrical companies from various countries around the world have also launched various products based on PWM control strategies, which cover a wide range of fields and play a significant role in improving the efficiency of electricity utilization.

Table2.1 Classification Table

classification basis	type
ways of storing energy on the DC side	voltage type rectifiers
	current type rectifiers
switching modulation methods	soft switching modulation
	hard switching modulation

2.2 Review Research on PWM rectifier topology and mathematical model

PWM rectifiers can be categorized into two main types—voltage type and current type—based on the distinct DC side energy storage components they utilize. In different application scenarios, the academic community has different research focuses on the topology structure of PWM rectifiers. In low-power applications, focus on reducing switch losses and improving DC side performance. For high-power applications, parallel current type PWM rectifiers or series voltage type PWM rectifiers are used to improve the equivalent switching frequency and the quality of input grid side voltage and current.

By considering the topological configuration, differentiation can be made between two distinct categories: voltage source type (VSR) and current source type (CSR). The disparity between these classifications is notable. Although both are rectification control systems, one operates in the form of constant voltage output and the other operates in the form of constant current output. There are significant differences in the topology and control methods between the two. Other classification forms can basically be classified into these two, so studying topological structures into these two types is very targeted. A voltage source PWM rectifier is connected in parallel with a capacitor on the DC side to store energy. This rectifier can be used as a voltage source, with stable output voltage and low impedance characteristics. The PWM rectifier of the current source has an inductor on the DC side, which stores energy and has the high impedance characteristics of the current source. However, in most cases, voltage source PWM rectifiers have a wider range of applications due to their faster corresponding speed and easier implementation than current source rectifiers. Due to differences in application scenarios and power levels, these two topologies have different research focuses. If the required rectifier power is relatively

low, the main focus is on the output performance on the DC side and minimizing the number of power switching devices. If the required power is relatively high, the research content should include the combination of rectifiers, multi-level topology, modulation technology of soft switching, etc.

The mathematical model is the first step in studying the control theory of PWM rectifiers. Summarizing the research work of previous scholars on PWM mathematical models, the research process of mathematical models here includes continuous and discrete dynamic mathematical models, high and low frequency time-domain dynamic models with time domain solutions, and novel reduced order small signal models. The most commonly used here is related coordinate transformation, which generally transforms the coupling type in the stationary coordinate system to the decoupling type in other coordinate systems and uses mathematical tools for analysis. Only after obtaining the relevant mathematical models can the control variables related to the research object be captured. Moreover, due to the different research focuses on PWM rectifiers, many forms of PWM rectifier models have been developed, such as Lagrange models and switch function models. At the same time, the mathematical methods that have developed mainly include Kirchhoff's law method, Tregen's theorem method, and Lagrange's equation method. Because Kirchhoff's law is relatively mature and commonly used in circuit analysis, it is also applied to power electronic analysis, becoming the most basic modeling method.

2.3 Research on PWM rectifier control technology

Diverse control strategies for PWM rectifiers have emerged over time, categorized into four main types: indirect current regulation, direct current regulation, direct power control, and nonlinear control, reflecting advancements in technology.

Table2.2 Control strategies Table

Serial Number	Control strategies
1	Amplitude and phase control
2	Direct current control
3	Direct power control
4	Nonlinear control

1. Amplitude and phase control

Amplitude and phase control, a form of indirect current regulation, governs the voltage equilibrium under steady-state conditions, as dictated by the system's steady-state mathematical model. In 1982, Busse Alfred et al. introduced a novel strategy for controlling grid-side current amplitude and phase in a three-phase full bridge PWM rectifier, employing controllable switches. This approach obviates the need for current sensor feedback and results in minimal steady-state input current harmonics during operation, ensuring favorable steady-state characteristics and a relatively straightforward circuit structure. Nonetheless, it exhibits comparatively subpar dynamic characteristics, slow response rates, and limited robustness, rendering it susceptible to external disturbances and parameter variations.

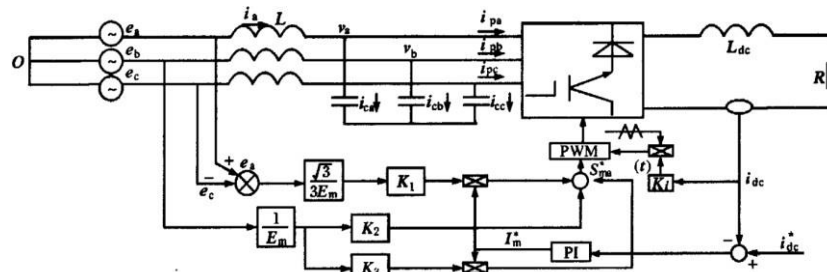


Figure 2.1 amplitude and phase control

2. Direct current regulation

Direct current regulation addresses the limitations of indirect current control by integrating a current loop to establish a dual closed-loop configuration, thereby enhancing the response and steady-state properties of input and output parameters and bolstering its dynamic and steady-state performance. This structure is widely used, and the control strategy of this article is also based on this structure for research. Peak current control, hysteresis current control, and predictive transient current control all use this structure.

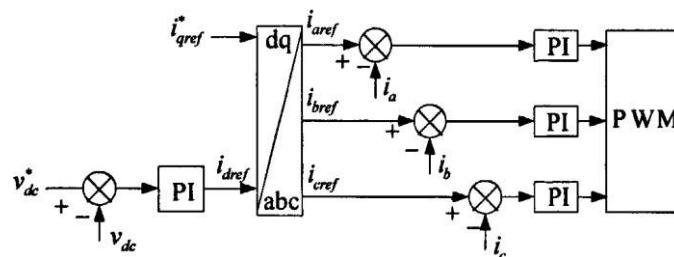


Figure 2.2 direct current regulation

3. Direct power control

Direct power control technology has developed rapidly and is widely used in practical applications and theoretical research.

Effectively managing the active and reactive power at the grid side to attain instantaneous current regulation entails manipulating the input current to optimize the active component while nullifying the reactive component. Its control structure is clean, has fast dynamic response, and a given power factor. The bus voltage output and power factor are stable and adjustable. Unlike the SVPWM control method, this method establishes a model that does not require coordinate transformation and eliminates the PWM modulation part. Therefore, the modeling results are concise, and the system has a high power factor and fast dynamic response. Moreover, compared with direct torque control, it reduces the sampling physical quantity, so the hardware structure is simple, the influence of motor parameters on the control is small, and high calculation accuracy can be achieved. Therefore, direct power control, as a new control technology for voltage source PWM rectifiers, can achieve the set performance indicators. Nonetheless, the modulation process in direct power control involves the adjustment of active and reactive power via hysteresis comparison, posing challenges in maintaining a constant switching frequency and introducing harmonic interference to the grid side. This complication escalates the complexity of selecting input filtering components.

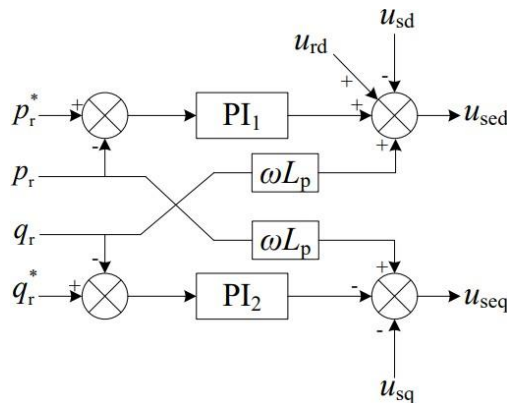


Figure 2.3 direct power control

4. Nonlinear control

Due to the fact that voltage source PWM rectifiers are nonlinear systems, the application of linear control methods can lead to a decrease in the dynamic response and stability of the system under large-scale disturbances. Treating the system as a small signal model and using linear methods to control the system is no longer suitable for this situation [8]. Hence, to enhance the rectifiers' control efficacy, using nonlinear

control theory or proposing novel control strategies to study voltage source PWM rectifiers has become a difficult and new hotspot in academic research.

Due to the fact that voltage source PWM rectifiers are nonlinear systems, linear control methods are applied. During significant disturbances, the system experiences a decline in both dynamic response and stability. Treating the system as a small signal model and using linear methods to control the system is no longer suitable for this situation. As such, to enhance the control performance of rectifiers, using nonlinear control theory or proposing novel control strategies to study voltage source PWM rectifiers has become a difficult and new hotspot in academic research.

(1) Variable Structure Control with Sliding Mode

Variable structure control with sliding mode finds broad application, particularly adept for dynamic nonlinear systems with time-varying characteristics, wherein nonlinearity manifests through control discontinuity. Compared with other control methods, this control strategy is applied to systems with unstable structures. In the process of dynamic changes, the control strategy model itself is variable, following the current state of the system and changing according to the control target time, so that the system can move on the set sliding surface trajectory and become stable. The switch of the rectifier is constantly switching, therefore, PWM rectifiers have nonlinear properties. Taking advantage of the advantages of sliding mode variable structure control, in a nonlinear system like PWM rectifiers, sliding mode control can make it independent of parameters and disturbances, including grid voltage, load parameters, and switching devices, and has strong robustness. However, its parameter design is quite difficult, and the sliding membrane parameters have a significant impact on control. Only by selecting the appropriate one can the system move on the sliding surface. Improper selection can easily cause vibration to the system, which may deviate from the sliding surface and lead to control failure.

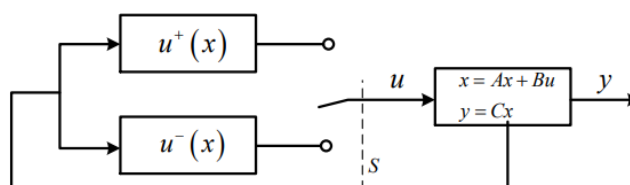


Figure 2.4 Variable Structure Control with Sliding Mode

(2) Feedback linearization control

Feedback exact linearization control, as the name suggests, is a method of converting nonlinear systems into linear system control, belonging to differential

geometry linearization decoupling control. Nonlinear systems generally cannot obtain analytical solutions. The mathematical analysis of this control method relies on differential geometry, starting from geometric or band number characteristics, combined with nonlinear states and feedback transformations, to achieve accurate linearization of the system state variables. This simplifies the problem from nonlinear to linear, and the applicable methods also change from nonlinear to linear. The control methods for various linear systems are very mature, thus greatly reducing the difficulty of control. This method can accelerate the DC voltage response speed of the system, with good tracking performance and small current waveform. However, due to the complexity of calculation, it is difficult to find the optimal feedback control law. It requires the cooperation of a digital signal processor DSP with fast computing function or a powerful MCU, which increases the system cost.

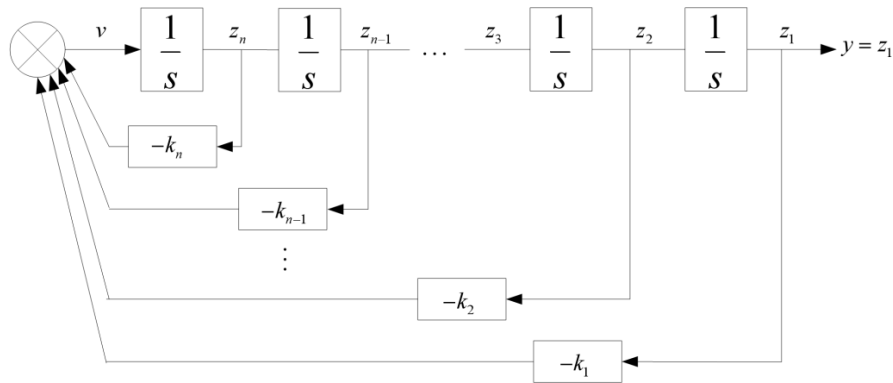


Figure 2.5 feedback linearization control

(3) Lyapunov stability theory control

In this theory, an initial scalar function is employed to represent the control object, with the value of this function diminishing over time during the closed-loop control design process. This theory was successfully applied in practice in the 1880s and can still perform closed-loop regulation on rectifiers under harsh working conditions. The theory formulates a Lyapunov function by leveraging the status of energy storage components, and uses the Lyapunov stability criterion and mathematical model of rectifiers, combined with the constraint conditions of SVPWM, to control the stability of the system.

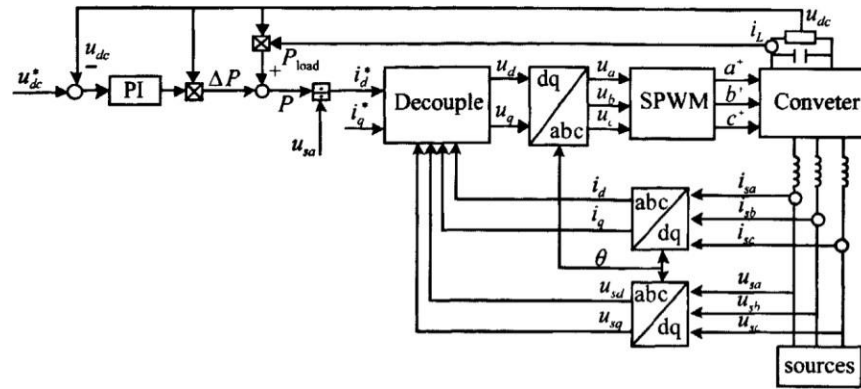


Figure 2.6 Lyapunov stability theory control

2.4 Summary

This chapter mainly introduces the development of three-phase rectifiers. An introduction was made to the corresponding control methods for rectifiers. This is beneficial for the understanding and analysis of three-phase rectifiers in the future.

CHAPTER 3

RESEARCH METHODOLOGY

3.1 Introduction

The arrangement of components for a three-phase voltage-type PWM rectifier is illustrated in Figure 3.1. Obviously, PWM rectifiers can operate in both inverter and rectifier states, therefore they have the characteristics of bidirectional energy flow and four quadrant operation. This graduation project mainly studies the working characteristics of rectifiers in inverter states.

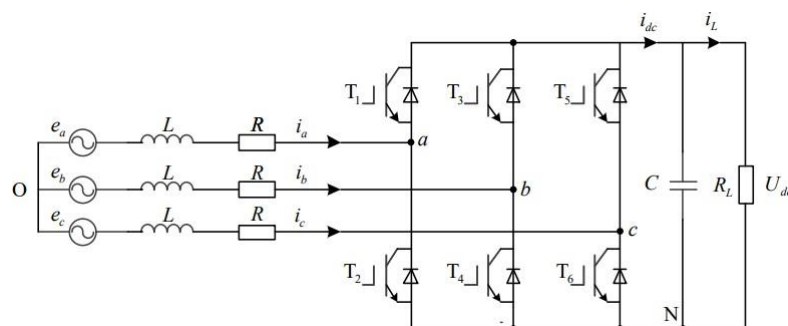


Figure 3.1 Three phase voltage type PWM rectifier circuit

Among them, T1~T6 are power switching devices IGBT, and each switching tube is connected in parallel with a freewheeling diode to complete the freewheeling of the inductor current when the power tube is not conducting. The inductance denoted as L serves as a filtering component situated on the AC side, facilitating energy transfer and mitigating harmonics produced by the high-frequency switching of power transistors. Meanwhile, resistance, labeled as R , represents the load resistance at the output. Additionally, C represents the DC bus voltage, serving to stabilize the DC bus voltage and attenuate high-frequency harmonics within the voltage waveform.

Figure 3.2 shows the model circuit of a PWM inverter. As shown in the figure: The circuit model for the PWM inverter comprises three distinct segments: the AC circuit, the inverter bridge circuit, and the DC circuit. Within the AC circuit, components primarily include the inductance L and the AC electromotive force e . As for the inverter bridge circuit, it can be categorized into two variants: voltage type and current type; The DC path contains electromotive force eL , etc.

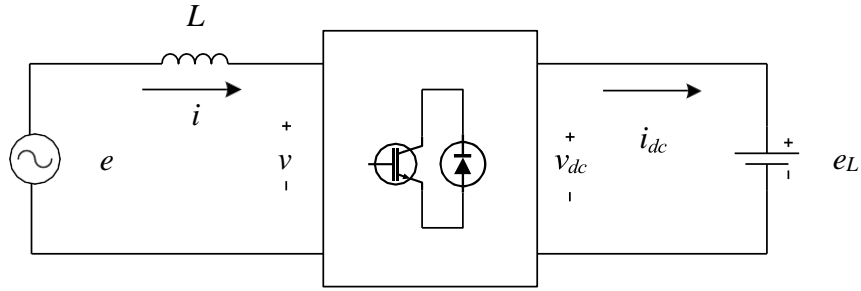


Figure 3.2 Model circuit of rectifier

According to theoretical analysis, assuming that the bridge does not consume energy, it can be inferred from the power conservation relationship between the AC and DC sides that

$$iv = i_{dc}v_{dc} \quad (3.1)$$

In the formula, i and v respectively represent the current and voltage in the AC circuit; i_{dc} and v_{dc} respectively represent the current and voltage in the DC path.

It is not difficult to see from the equation that to control the DC side of the model circuit, one can start from its AC side, and the opposite is also true. Next, starting from the grid side of the PWM inverter model circuit, we will analyze its operating status and control principle. When the PWM inverter operates in a steady-state state, the vector relationship on its AC side is shown in Figure 3.3.

In order to simplify the analysis, only the PWM fundamental component is considered and the influence of resistance on the AC side is ignored. From Figure 3-3, it can be analyzed as follows: to clarify the relationship between vectors, it is necessary to select a reference object. In the selection of reference objects, the electromotive force vector E of the AC power grid can be used as a reference object. In order to enable the PWM inverter to operate in four quadrants, it can be achieved by controlling the voltage vector V . The presence of inductance prevents a sudden change in current. In theory, $|I|$ remains constant, so $|V_L| = \omega L |I|$ also does not change. From this perspective, the endpoint motion trajectory of the inverter AC voltage vector V is a circle with a radius of $|V_L|$. Assuming the voltage endpoint is at point A, the current vector I lags behind the vector E 90° . At this time, on the AC side of the PWM inverter, its impedance is purely inductive, as shown in Figure 3.3a); The voltage vector V continues to operate, and when its endpoint coincides with point B, the current vector I and the electromotive force vector E have the same phase. The grid side of the three-phase inverter has a positive resistance characteristic, as shown in Figure 3.3b); The voltage vector V follows a circular trajectory from point C forward, and the phase

difference between the grid voltage E and the current vector I is $\pi/2$. The grid side of the three-phase inverter exhibits pure capacitance, as shown in Figure 3.3c); The voltage vector V continues to rotate along a circular trajectory to point D. At this point, the phase of the current vector I and the phase of the electromotive force vector E show a difference of π . The grid side characteristic of the three-phase inverter is negative resistance, as shown in Figure 3.3d). When PWM inverters operate in four quadrants, there are four special operating state points, namely A, B, C, and D. Through in-depth analysis of these four points, it can be concluded that PWM inverters have the following operating rules:

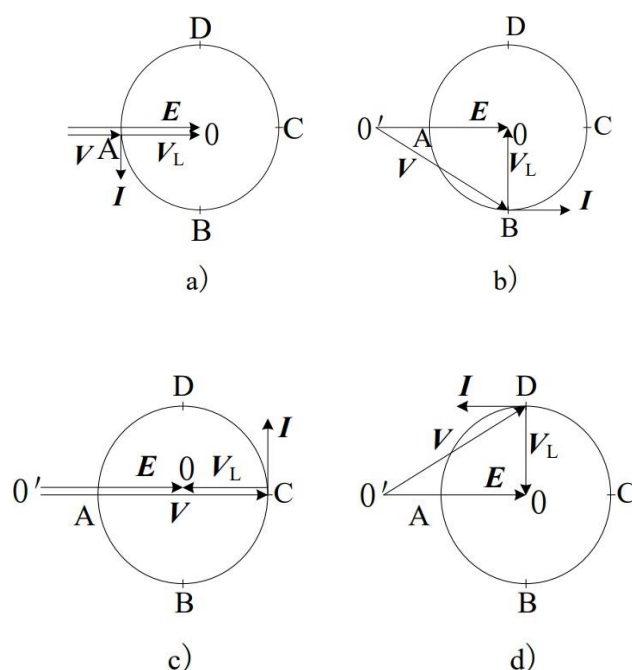


Figure 3.3 Steady State Vector Relationship on AC Side of PWM Rectifier

1. When the voltage vector V traverses the arc between points A and B, the PWM inverter enters the inverter mode. In this scenario, the three-phase inverter system must uptake active power and inductive reactive power from the grid side, facilitating energy transfer from the grid side to the DC side. It's essential to highlight that when the voltage vector V reaches point B, the power factor angle of the PWM inverter is 0, thereby achieving unit power factor control. Conversely, at point A, the PWM inverter solely absorbs inductive reactive power from the power grid without consuming active power.

2. As the voltage vector V progresses along the arc from points B to C, the PWM inverter transitions to the inverter mode. During this phase, the three-phase inverter system is tasked with absorbing both active power and capacitive reactive

power from the grid side, while maintaining energy transmission from the grid side to the DC side. Upon reaching point C, the three-phase inverter ceases the transmission of active power, focusing solely on the transfer of reactive power from the grid side.

3. Moving along the arc from points C to D, the operation of the system undergoes a reversal. Energy transfer now originates from the DC side towards the AC side, with the grid side absorbing both active power and capacitive reactive power from the DC side. Consequently, energy flows from the DC side to the grid side. Upon reaching point D, the PWM inverters can achieve active control with unit power factor.

4. Advancing along the arc from points D to A, the PWM rectifier enters an active inverter state. In this phase, the grid side of the inverter absorbs active and inductive reactive power from the DC side, driving energy flow from the DC side to the AC side.

3.2 Mathematical models

To streamline the mathematical model derivation process and ease the analysis of voltage source PWM inverters, the following assumptions need to be made:

1. The grid side is represented by a symmetrical three-phase voltage source, featuring uniform amplitudes and 120-degree phase disparities, with an ideal sinusoidal waveform.
2. Without considering the saturation of the filtering inductance L on the three-phase AC input side, the equivalent internal resistance values are equal, the inductance characteristics are linear, and the inductance values of each phase are equal.
3. The power switching transistor is considered an ideal switch, without considering the switching transition process and power loss. Its on/off state can be described by the switching function, regardless of the impact of dead zones on the system.
4. In terms of fundamental frequency manifestation, the switching tube exhibits a significantly higher switching frequency compared to that of the power grid.

Given the preceding presumptions, the switching function serves to delineate the status of the switching transistor. Thus, within this framework, the depiction of the unipolar binary logic switching function S_k is outlined as follows:

$$S_k = \begin{cases} 1, & \text{Upper bridge arm conduction, lower bridge arm shutdown} \\ 0, & \text{Lower bridge arm conduction, upper bridge arm shutdown} \end{cases} \quad k=a,b,c \quad (3.2)$$

Write the Kirchhoff voltage equation for the a, b, and c phase circuits in Figure 3-2 to obtain the mathematical model in the three-phase stationary coordinate system:

$$\left\{ \begin{array}{l} L \frac{di_a}{dt} = u_a - \frac{U_{dc}(2S_a - S_b - S_c)}{3} \\ L \frac{di_b}{dt} = u_b - \frac{U_{dc}(-S_a + 2S_b - S_c)}{3} \\ L \frac{di_c}{dt} = u_c - \frac{U_{dc}(-S_a - S_b + 2S_c)}{3} \\ C \frac{du_{dc}}{dt} = i_a S_a + i_b S_b + i_c S_c - i_L \end{array} \right. \quad (3.3)$$

The mathematical model in three-phase ABC coordinate system has the characteristics of clear and explicit physical meaning. However, due to the fact that each physical quantity at the grid side input of the voltage source PWM inverter is a time variable, it makes the control design of the system difficult. Therefore, transforming the abc coordinate system into the $\alpha\beta$ coordinate system simplifies the mathematical model and facilitates system control design.

In the $\alpha\beta$ coordinate system, with the help of coordinate transformation, the mathematical model of the system is:

$$\left\{ \begin{array}{l} L \frac{di_\alpha}{dt} = u_\alpha - S_\alpha U_{dc} \\ L \frac{di_\beta}{dt} = u_\beta - S_\beta U_{dc} \\ C \frac{du_{dc}}{dt} = \frac{3}{2}(i_\alpha S_\alpha + i_\beta S_\beta) - i_L \end{array} \right. \quad (3.4)$$

Typically, the Park transformation is employed to convert the $\alpha\beta$ two-phase stationary coordinate system into the dq two-phase rotating coordinate system. By implementing the Park transformation to the subsequent equation, the mathematical representation of the system in the dq rotating coordinate system can be derived as follows:

$$\left\{ \begin{array}{l} L \frac{di_d}{dt} = u_d - S_d U_{dc} \\ L \frac{di_q}{dt} = u_q - S_q U_{dc} \\ C \frac{du_{dc}}{dt} = \frac{3}{2}(i_d S_d + i_q S_q) - i_L \end{array} \right. \quad (3.5)$$

Figure 3.4 illustrates the mathematical model diagram of the system depicted in the dq coordinate system.

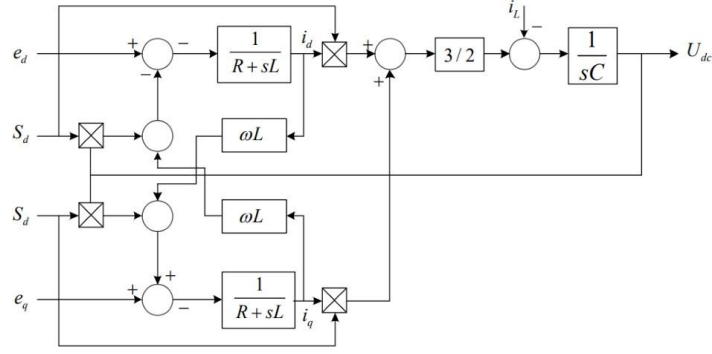


Figure 3.4 dq mathematical model

3.3 Analysis of Double Closed Loop Linear Control

Below presents the mathematical formulation of a voltage source PWM inverter within the dq coordinate system.

$$\begin{bmatrix} e_d \\ e_q \end{bmatrix} = \begin{bmatrix} Lp + R & -\omega L \\ \omega L & Lp + R \end{bmatrix} \begin{bmatrix} i_d \\ i_q \end{bmatrix} + \begin{bmatrix} u_d \\ u_q \end{bmatrix} \quad (3.6)$$

The dq model highlights the interdependence among the dq-axis variables of the current in a three-phase voltage source PWM inverter, complicating controller design. To mitigate this interdependence and streamline controller design, a feedforward decoupling control approach is implemented to untangle the current dq component. A linear control strategy is then utilized to implement PI control in the current controller. By regulating the magnitude of the AC current dq component, the input active and reactive power can be managed. After applying PI control, the u_d and u_q equations of the current controller are:

$$\begin{cases} u_d = -(K_{ip} + \frac{K_{il}}{s})(i_d^* - i_d) + \omega L i_q + e_d \\ u_q = -(K_{iq} + \frac{K_{il}}{s})(i_q^* - i_q) - \omega L i_d + e_q \end{cases} \quad (3.7)$$

Combining the above two equations, we can obtain:

$$P \begin{bmatrix} i_d \\ i_q \end{bmatrix} = \begin{bmatrix} -\left[R - \left(K_{ip} + \frac{K_d}{s} \right) \right] / L & 0 \\ 0 & -\left[R - \left(K_{iq} + \frac{K_d}{s} \right) \right] / L \end{bmatrix} \begin{bmatrix} i_d \\ i_q \end{bmatrix} - \frac{1}{L} \begin{bmatrix} K_{ip} + \frac{K_d}{s} \\ K_{iq} + \frac{K_d}{s} \end{bmatrix} \begin{bmatrix} i_d^* \\ i_q^* \end{bmatrix} \quad (3.8)$$

Observing the state equation provided above, it becomes apparent that active and reactive currents are now decoupled, enabling independent and precise control over each. Based on the equation, the system structure of voltage source PWM inverter dq decoupling current feedforward control is obtained, as shown in Figure 3.5.

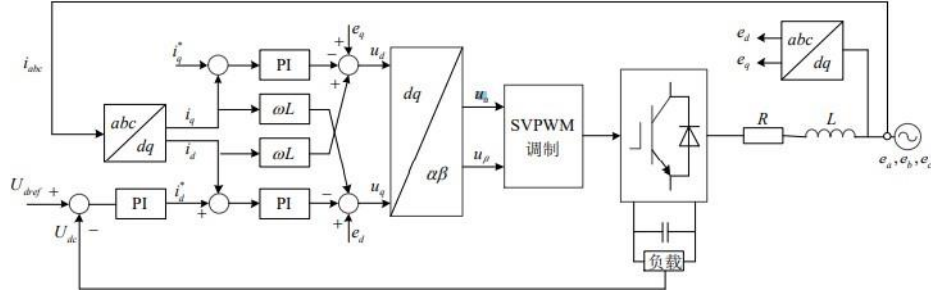


Figure 3.5 Structure of feedforward decoupling PI control system

3.3.1 PI current inner loop design

Upon scrutinizing the inner workings of the current system with the disentanglement of active and reactive currents, observations unveil the presence of signal delay and a minor inertia component within the system during sampling. The schematic depicting the transfer function structure of the current's inner loop is showcased in Figure 3.6. Within this diagram, T_s represents the sampling period of the current's inner loop, K_{PWM} denotes the equivalent gain of the inverter bridge circuit, with its value contingent upon the modulation technique employed. When using SVPWM modulation, K_{PWM} is $1/\sqrt{3}$.

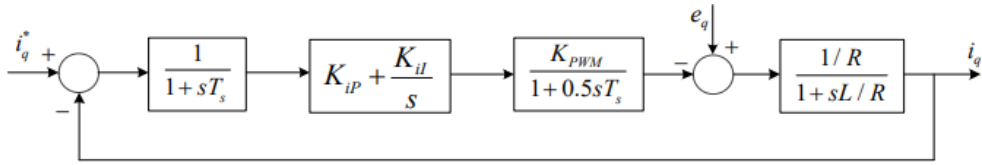


Figure 3.6 Current Inner Ring Structure Diagram

For the sake of simplicity and without considering the influence of e_q changes, the transfer function of the PI controller is transformed into a zero pole expression, as shown in the following equation:

$$K_{iP} + \frac{K_{iP}}{s} = K_{iP} \frac{\tau_i s + 1}{\tau_i s} \quad (\tau_i = \frac{K_{iP}}{K_{iI}}) \quad (3.9)$$

Merge the small time constant T_s and $0.5T_s$ links to obtain a simplified structural diagram of the inner loop, as shown in Figure 3.7:

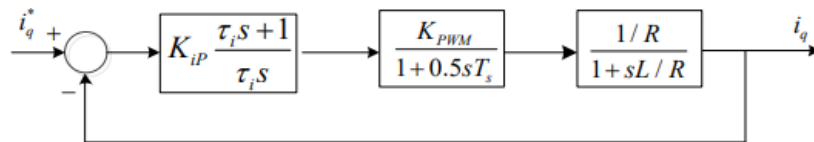


Figure 3.7 Simplified current inner loop structure diagram

To attain rapid dynamic response in the current loop, a conventional Y-type system configuration is adopted for the current loop system design. As depicted in the

graphical representation provided in Figure 3.7, the poles of the current loop regulation mechanism can be shifted by the zero point of the PI controller, thus altering the dynamic characteristics of the system.

$$\tau_i = \frac{L}{R} \quad (3.10)$$

The corrected current inner loop open-loop transfer function is:

$$W_{oi} = \frac{K_{iP}K_{PWM}}{R\tau_i s(1.5T_s + 1)} \quad (3.11)$$

According to the parameter tuning relationship of a typical Y-type system, when the damping ratio ξ is set to 0.707, the system performance is optimal, which includes:

$$\frac{1.5T_s K_{iP} K_{PWM}}{R\tau_i} = \frac{1}{2} \quad (3.12)$$

Obtain the PI control tuning coefficient:

$$\left\{ \begin{array}{l} K_{iP} = \frac{R\tau_i}{3T_s K_{PWM}} \\ K_{iI} = \frac{K_{iP}}{T_i} = \frac{R\tau_i}{3T_s K_{PWM} T_i} \end{array} \right. \quad (3.13)$$

As shown in the figure, the closed-loop transfer function of the current loop is:

$$W_{ci}(s) = \frac{1}{R\tau_i} \frac{1}{1 + \frac{K_{iP} K_{PWM}}{R\tau_i} s + \frac{1.5T_s R\tau_i}{K_{iP} K_{PWM}} s^2} \quad (3.14)$$

In instances where the switching frequency is sufficiently high, namely when T_s is minimized and the coefficient of the s^2 term is substantially inferior to that of the s term, the s^2 term becomes negligible. Consequently, the closed-loop transfer function of the current loop can be further streamlined as follows:

$$W_{ci}(s) \approx \frac{1}{R\tau_i} \frac{1}{1 + \frac{K_{iP} K_{PWM}}{R\tau_i} s} \quad (3.15)$$

Analysis of the equation reveals that if one opts for the conventional H-type system when devising the current inner loop, the current loop can be likened to a primary-order inertial link with an inertial time constant equivalent to $3T_s$.

Furthermore, provided that the switching frequency attains a satisfactory pace, the current loop exhibits a swift dynamic response.

3.3.2 PI voltage outer loop design

The approach for designing the voltage outer loop PI controller mirrors that of the current inner loop, as both aim to stabilize the output terminal voltage and synchronize with the electromotive force of the three-phase power grid:

$$\begin{cases} e_a = E_m \cos \omega t \\ e = E \cos(\omega t - 120^\circ) \\ e^b = E^m \cos(\omega t + 120^\circ) \\ e^c = E^m \cos(\omega t + 120^\circ) \end{cases} \quad (3.16)$$

To simplify the design of the control system, disregarding the PWM harmonic components and high-frequency components of the switching function, and emphasizing unit power factor sinusoidal current control, the input current is outlined as follows:

$$\begin{cases} i_a = I_m \cos \omega t \\ i_b = I_m \cos(\omega t - 120^\circ) \\ i^c = I^m \cos(\omega t + 120^\circ) \\ i^c = I^m \cos(\omega t + 120^\circ) \end{cases} \quad (3.17)$$

Through the mathematical model of voltage source PWM inverter, it is known that:

$$I_{dc} = i_a s_a + i_b s_b + i_c s_c \quad (3.18)$$

United can obtain:

$$I_{dc} = 0.75 m I_m \cos \theta \quad (3.19)$$

According to the above equation, the voltage outer loop regulator structure of the voltage source PWM inverter is shown in Figure 3.8.

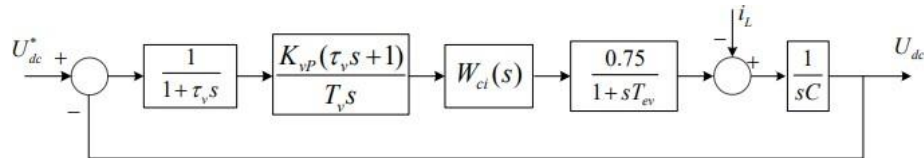


Figure 3.8 Voltage outer loop control structure

Further simplify the structure of the voltage controller by combining the voltage sampling small inertia time constant τ_v and the equivalent small time constant $3T_v$ of the current loop. If the change in load current i_L is not considered, the voltage outer loop can be simplified as shown in Figure 3.9.

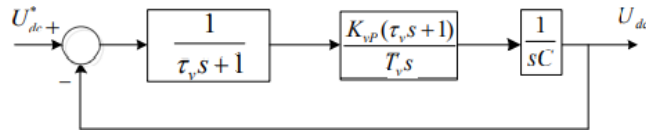


Figure 3.9 Simplified controller structure for voltage outer loop

Considering the robustness of the system, design a voltage regulator for a typical Type II system, analyze Figures 3.9, and obtain the open-loop transfer function of the voltage loop:

$$W_{ov} = \frac{0.75K_{vp}(T_v s + 1)}{CT_v s^2(T_{pv} s + 1)} \quad (3.20)$$

Considering the voltage outer loop control system's resistance to interference and its ability to track signals accurately, it is common in engineering to take the intermediate frequency width $h\nu=5$. Therefore, it can be inferred that the gain of the voltage loop PI regulator is:

$$\begin{cases} K_{vp} = \frac{4C}{\tau_v + 3T_s} \\ K_{vi} = \frac{K_p}{T_s} = \frac{4C}{5(\tau_v + 3T_s)^2} \end{cases} \quad (3.21)$$

3.4 Design of inductance and capacitor

3.4.1 Design of AC side inductance

The presence of inductance L on the AC side significantly influences the operational effectiveness of the entire primary circuit. Its main function is to filter out the AC side switch ripple, isolate the AC side voltage from the grid electromotive force, achieve bidirectional energy transmission, and make the converter a circuit with Boost characteristics.

The size of the grid side inductance is directly related to the size of the ripple in the input circuit. Enhancing the inductance can elevate the circuit's quality factor and diminish the harmonic elements within the power supply current. However, this adjustment concurrently diminishes the circuit's dynamic responsiveness. The value of inductance mainly considers the following points:

1. Under different operating conditions of the inverter, take the maximum inductance value of the system during normal operation;
2. Take the minimum value of inductance within the allowable AC current ripple range of the system;

3. The smaller the inductance, the faster it can track the current, so when selecting the inductance value, it is necessary to refer to the transient current tracking index;
4. The smaller the inductance, the lower the cost. It is necessary to minimize the inductance as much as possible without affecting system performance.

There are two main methods for designing inductors:

1. Design of inductance when meeting power steady-state indicators;
2. Design of inductance to meet transient current tracking criteria.

Below, the two methods will be introduced separately.

1. Design of inductance when meeting power steady-state indicators

Figure 3.10 illustrates the vector relationship diagram corresponding to the AC side of a three-phase voltage source PWM inverter under steady-state conditions. It primarily focuses on the fundamental sinusoidal electrical parameter while omitting any reference to the AC side resistance R of the inverter. Within the diagram, U denotes the input voltage on the AC side, U_L signifies the inductance voltage on the AC side, U_{AB} represents the AC voltage of the input bridge inverter, and I_N denotes the input current on the AC side.

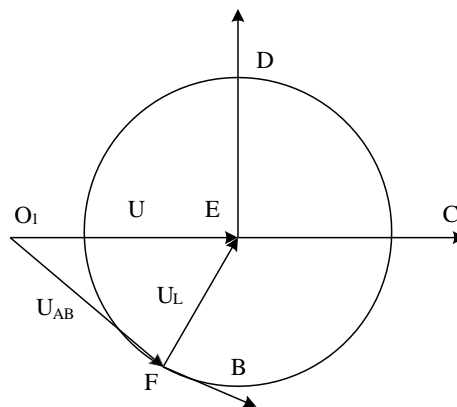


Figure 3.10 Diagram of steady-state vector relationship on the AC side

At the point C operation, the minimal threshold for inductance is reached, defining the upper boundary for inductance L .

$$L \leq \frac{U_{dc} - U_m}{\omega I_m} \quad (3.22)$$

2. Inductor design that meets the requirements of transient current tracking indicators

The design of the AC side inductor L should not only meet the requirements of power steady-state indicators, but also have the ability to quickly track current. In practical applications, the designed inductance value should be able to achieve both fast current tracking and suppression of harmonic current pulsation, which requires

meeting the requirements of transient current tracking indicators. During SVPWM modulation, the current experiences its highest rate of change amidst the zero-crossing region of the input current on the AC side. To adeptly trace the current, it's advantageous to minimize the inductance value. Conversely, at the zenith of the input current on the AC side, harmonics reach their pinnacle. In order to suppress the harmonic current, the inductance value should be as large as possible. Finally, by searching relevant literature, the lower limit of inductance value is obtained as follows:

$$L \geq \frac{U_m T_s (U_{dc} - U_N)}{\Delta i_{\max} U_{dc}} \quad (3.23)$$

3.4.2 Design of DC side capacitor

The DC side capacitor C is an intermediate link in balancing energy, and the selection of the capacitor C for the DC side is intimately tied to the features and safety aspects of the inverter system. The main reason for voltage fluctuations in capacitors is the energy deviation between input and output. Choosing a larger capacitor can effectively suppress voltage fluctuations, but excessive capacitor selection can affect the dynamic response performance of the circuit. Due to the addition of a secondary filter on the intermediate DC side, the value of the DC side capacitor C mainly depends on the changes in leakage inductance energy storage on the AC side.

When designing, not only should the dynamic tracking performance of the DC output voltage be considered, but also the filtering stability performance of the bus voltage should be ensured. Under these considerations, the final selection of capacitors should meet the following requirements:

$$\frac{i_{dc} T_s}{2\Delta v_{dc}} \leq C \leq \frac{t_r}{R_L \ln \frac{i_{dcm} R_L - v_{dc \min}}{i_{dc} R_L - v_{dc}}} \quad (3.24)$$

In the formula, ΔV_{dc} is the output voltage ripple; The step response time of the output voltage of t_r ; I_{dc} is the load current; I_{dcm} is the maximum value when the load current fluctuates; $V_{dc \min}$ is the minimum value when the output voltage fluctuates; R_L is the output load.

Finally, after selection, simulation verification should be carried out to ensure the following criteria. If not met, adjust the size of the capacitor appropriately:

(1) The stability of the intermediate DC circuit's voltage is maintained, ensuring that its peak-to-peak fluctuation does not surpass the designated permissible limit.

(2) The continuity of the intermediate DC circuit's current remains uninterrupted, with its peak-to-peak fluctuation adhering to the prescribed allowable threshold.

(3) Minimizing losses in the intermediate DC circuit is imperative.

(4) The stability of the entire system should remain unaffected by the chosen capacitor's parameters.

(5) It is essential to effectively mitigate transient phenomena on the DC side to uphold system stability.

3.4.3 Selection of Power Electronic Switch

Given the merits of IGBTs, including uncomplicated drive circuits, straightforward protection measures, robust reliability, and capacity for high-power operation, they have been chosen as the switching devices for the three-phase PWM inverter in this particular design. The selection is mainly based on the rated voltage v_{ce} and rated conduction current i_{ce} between the collector and emitter.

The design of rated voltage v_{ce} and rated current i_{ce} should take into account their respective voltage and current ripple, and leave sufficient margin. Set a voltage and current ripple of 20%, and the values of rated voltage v_{ce_IGBT} and rated current i_{ce_IGBT} are:

$$v_{ce_IGBT} = 1.2v_{dc} = 900V \quad (3.25)$$

$$i_{ce_IGBT} = 1.2 \times \sqrt{2}i_{Ln} = 77A \quad (3.26)$$

3.5 Summary

This chapter briefly introduces the basic working principle of PWM rectifiers, and based on this, provides a detailed explanation of the different switching modes of three-phase VSRs and their corresponding rectifier operation, discusses the engineering implementation of a voltage type PWM rectifier with dual closed-loop control, and designs the voltage type PWM rectifier from a hardware circuit perspective.

CHAPTER 4

RESULTS AND DISCUSSIONS

4.1 Introduction

MATLAB is now the most widely used software in the world because it combines the advantages of other software, such as ease of use and usability.

MATLAB is a powerful comprehensive software with high efficiency in programming, and its ability to use graphical functions is very powerful compared to other software. For our profession, the most important module in MATLAB software is SIMULINK, because if we want to implement a certain design, we must first obtain the parameters we want in the simulation system before we can do it in practice, so as to avoid wasting manpower and resources.

MATLAB can not only be used in many ways, but it is also very easy to learn. It is also very simple to draw using MATLAB. When using SIMULINK for simulation drawing, simply find the required components in the module library, drag them into the programming box, and then connect all the required components with wires to complete the simulation drawing. This can simplify the operation and programming, making it more convenient for users to use.

The Simulation parameters table is as follows:

Table4.1 Simulation parameters

Parameter	Numerical value
AC voltage	220V, 50Hz
DC Voltage	800V
Input harmonic current	<5%
Power factor	>0.99
Power level	5kW
Network side inductance	20mH
DC capacitor	4mF

4.2 Simulation Model Building

The simulation model of three-phase PWM rectifier in SIMULINK environment is shown in Figure 4.1.

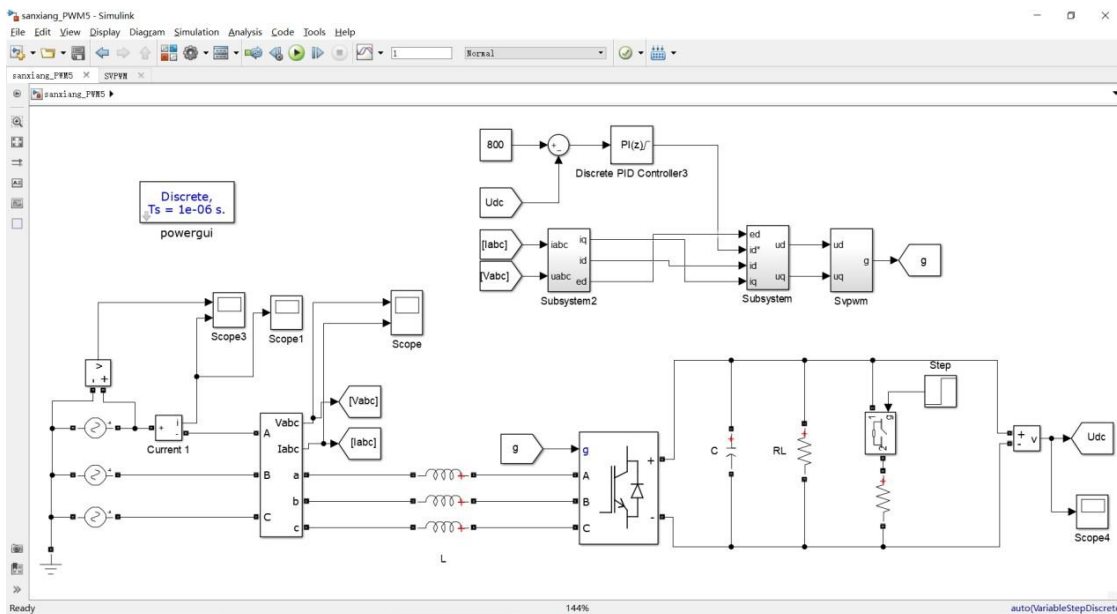


Figure 4.1 Simulation Model

Decoupling control is shown in Figure 4.2.

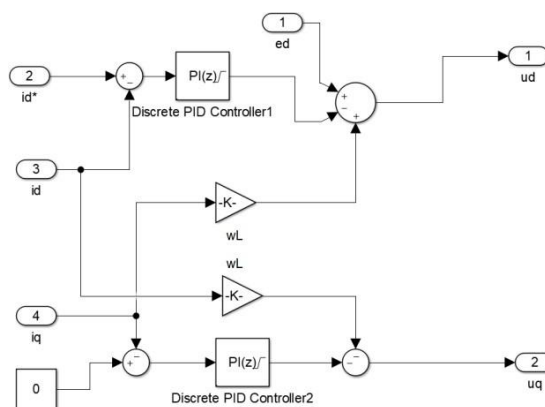


Figure 4.2 Decoupling Control

The phase-locked loop and coordinate transformation are shown in Figure 4.3.

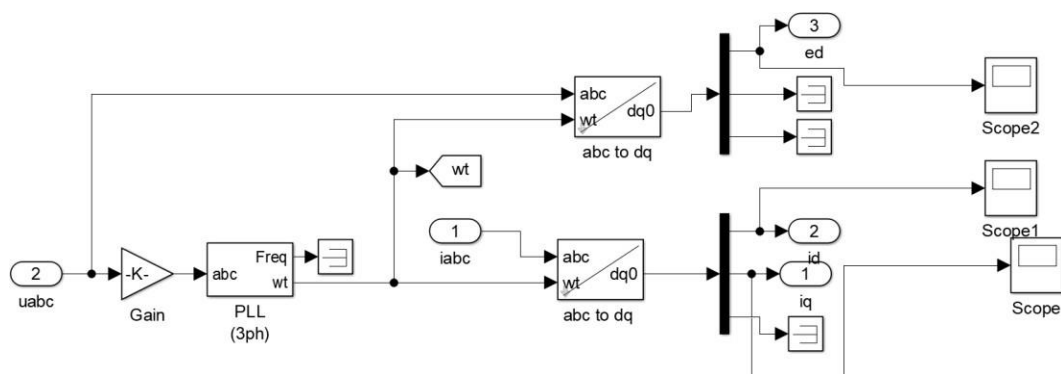
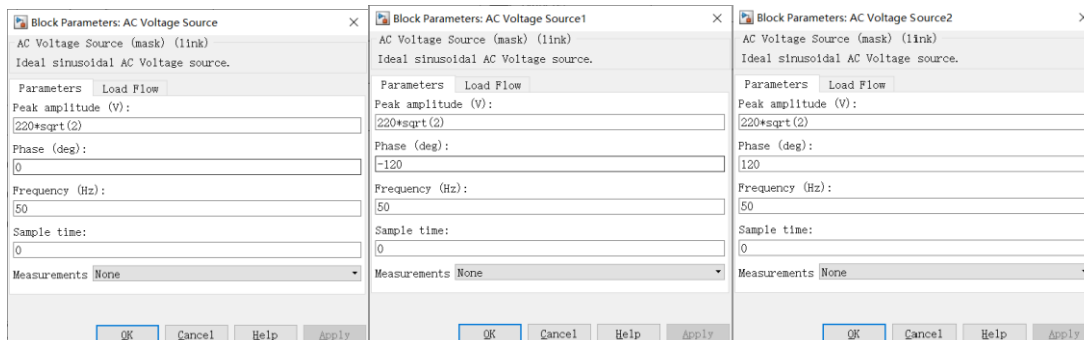
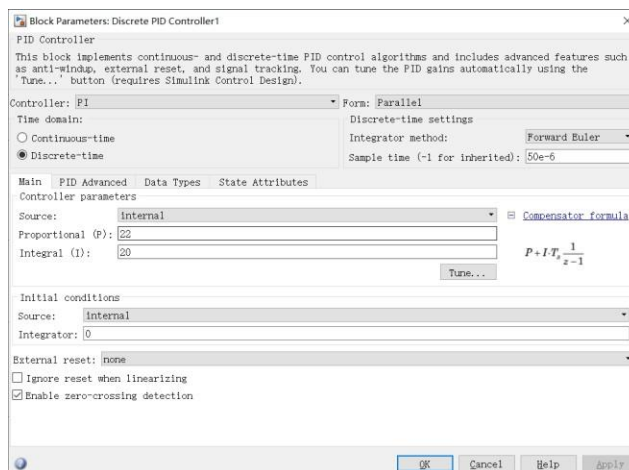


Figure 4.3 Phase Locked Loop and Coordinate Transformation

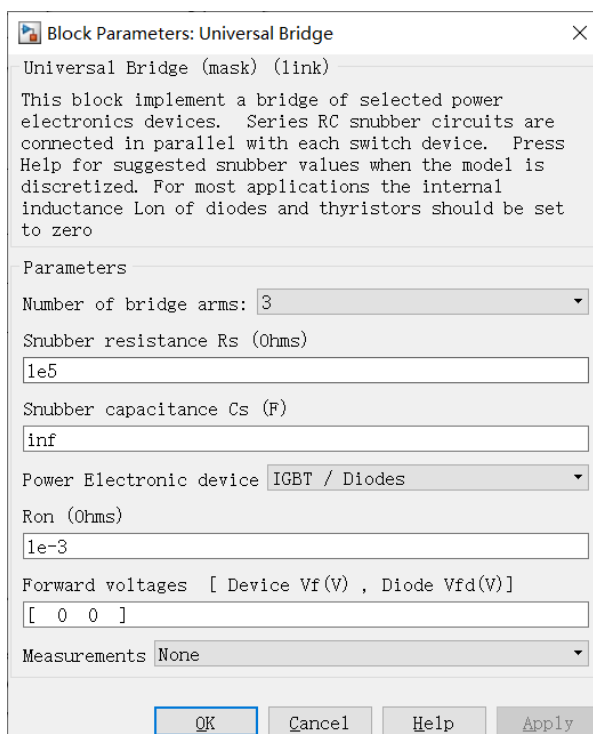
The three-phase voltage phase voltage is 220V, as shown in the following figure



The current inner loop PI parameters are set as follows:



The parameter settings for IGBT are as follows, which are the default parameters:



The SVPWM model is shown in the following figure:

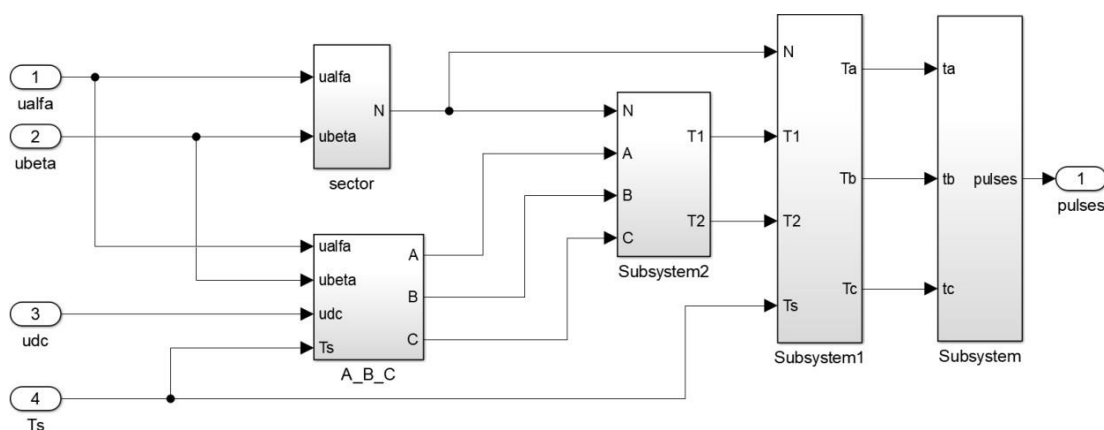


Figure 4.4 SVPWM model

4.3 Simulation waveform analysis

(1) Steady state simulation:

In the simulation, the DC bus voltage is controlled to 800V to ensure stable output voltage, and the reactive power is controlled to 0, that is, the given i_q is 0. Run the simulation, and the relevant waveform diagram is as follows:

The waveform of the DC bus voltage is shown in Figure 4.5, and it can be seen that the DC bus voltage is stable at the given value of 800V. Due to the role of a PI controller, the output voltage can closely follow the given voltage value, ensuring stable output voltage.

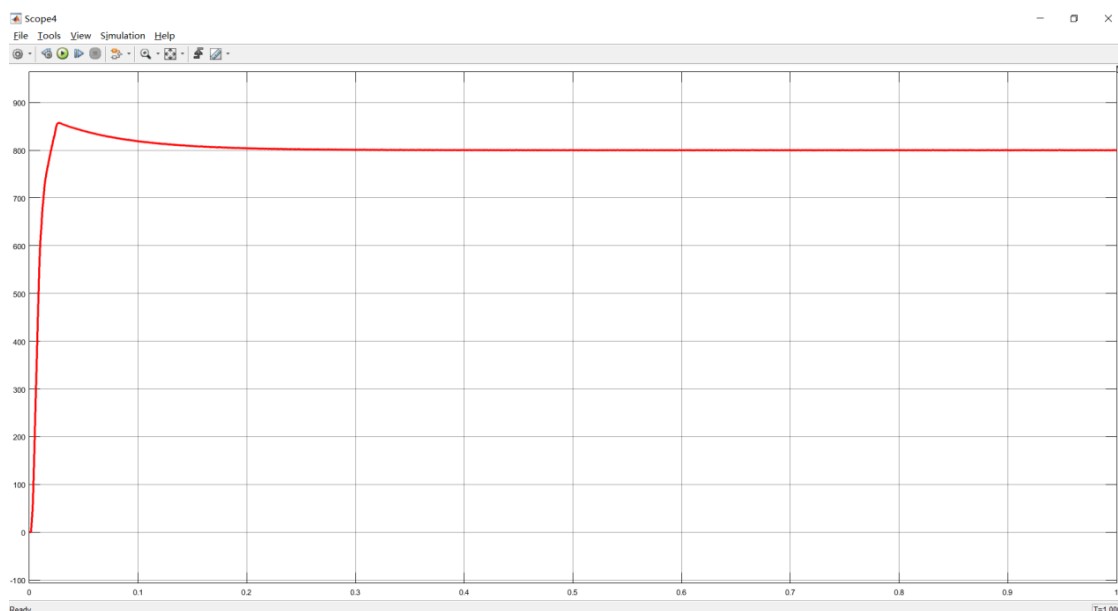


Figure 4.5 DC Bus Voltage

The graphical representation depicted in Figure 4.6 illustrates the voltage and current waveforms of phase A. Observing the graph reveals that the phase A voltage and current exhibit a phase difference of 0 degrees. Additionally, when the converter

operates at a unit power factor, the reactive power measures at 0, validating the efficacy of current inner loop control.

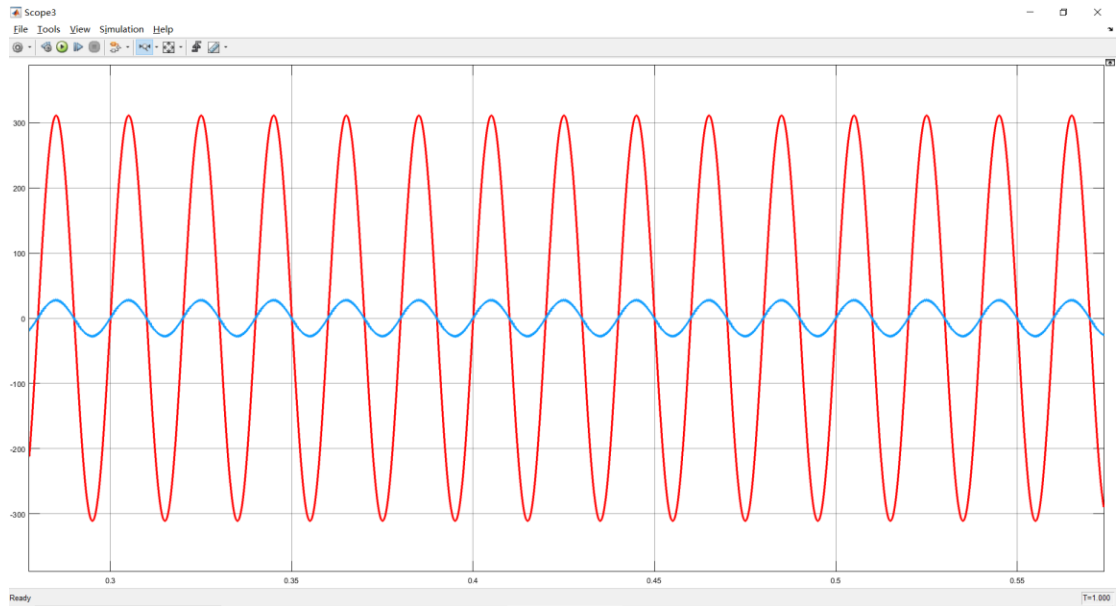


Figure 4.6 Waveform of A-phase Voltage and A-phase Current

The waveform of three-phase voltage and three-phase current is shown in Figure 4.7.

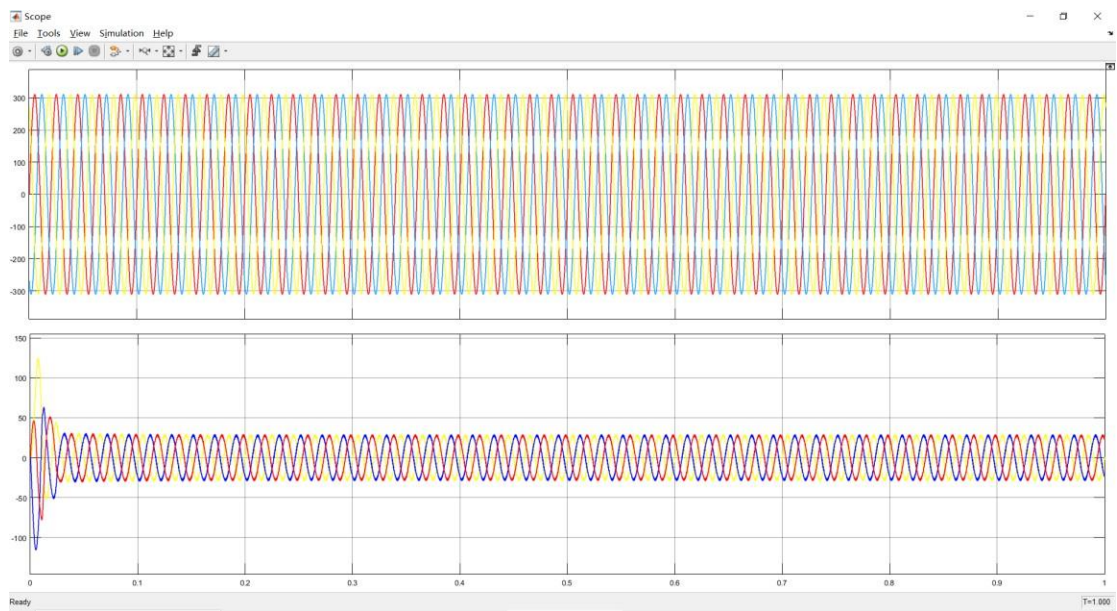


Figure 4.7 Three phase voltage and circuit waveform diagram

Figure 4.8 shows the THD diagram of phase A current, and it can be seen that the THD is only 4.28%, less than 5%, which meets the requirements of harmonic design in the power grid.



Figure 4.8 THD diagram of phase A

(2) Dynamic simulation:

In the simulation, the initial given resistance is 50Ω , and the transmission power is 12.8 kW; After 0.5 seconds, the output load resistance changes to 25Ω , the transmission power is 25.6 kW, the dynamic simulation of load jump is completed, and the reactive power is controlled to 0, that is, the given i_q is 0. Run the simulation, and the relevant waveform diagram is as follows:

Figures 4.9 illustrate the waveform depicting the DC bus voltage. Examination of the figures reveals the stabilization of the DC bus voltage at the predetermined value of 800V. After 0.5 seconds, the output voltage fluctuates due to load fluctuations, but quickly stabilizes to 800V due to the effect of the voltage outer loop.

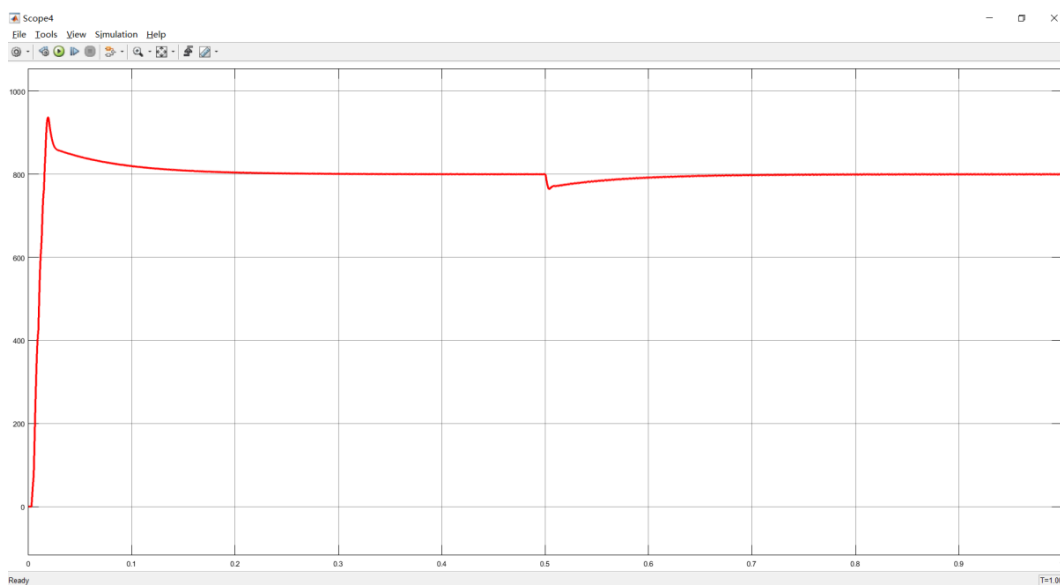


Figure 4.9 Waveform of DC Bus Voltage

In Figure 4.10, the graphical representation displays the voltage and current waveforms of phase A. Analysis of the figure reveals a phase difference of 0 degrees between phase A voltage and phase A current. Furthermore, the converter functions at a unit power factor with no reactive power. After 0.3 seconds, the current rapidly increases and the dynamic effect is good.

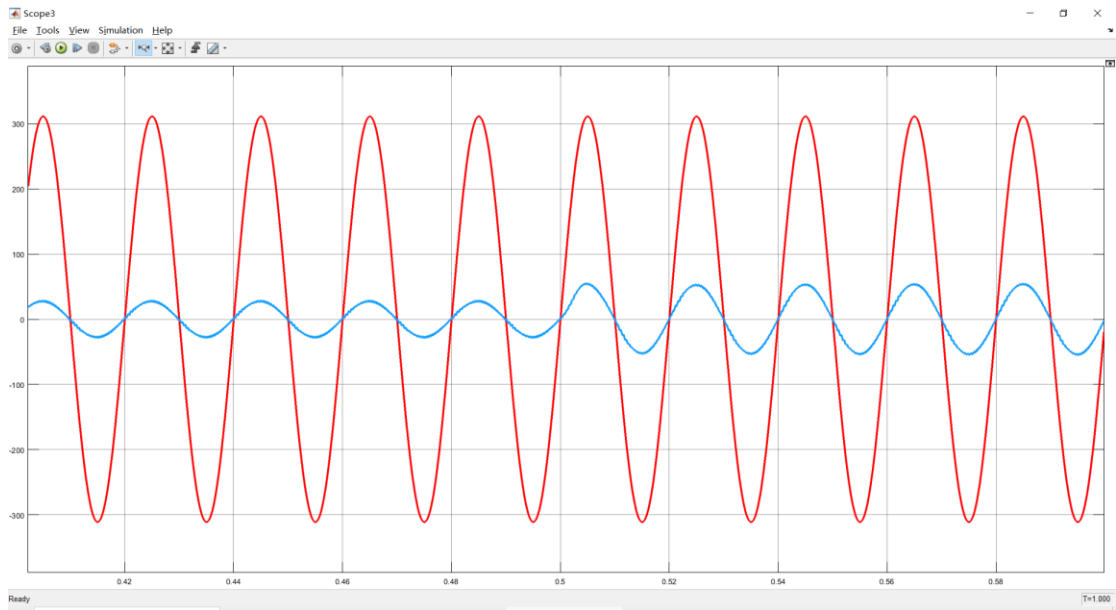


Figure 4.10 Waveform of A-phase Voltage and A-phase Current

Figure 4.11 displays the graphical representation of the voltage and current waveforms across all three phases.

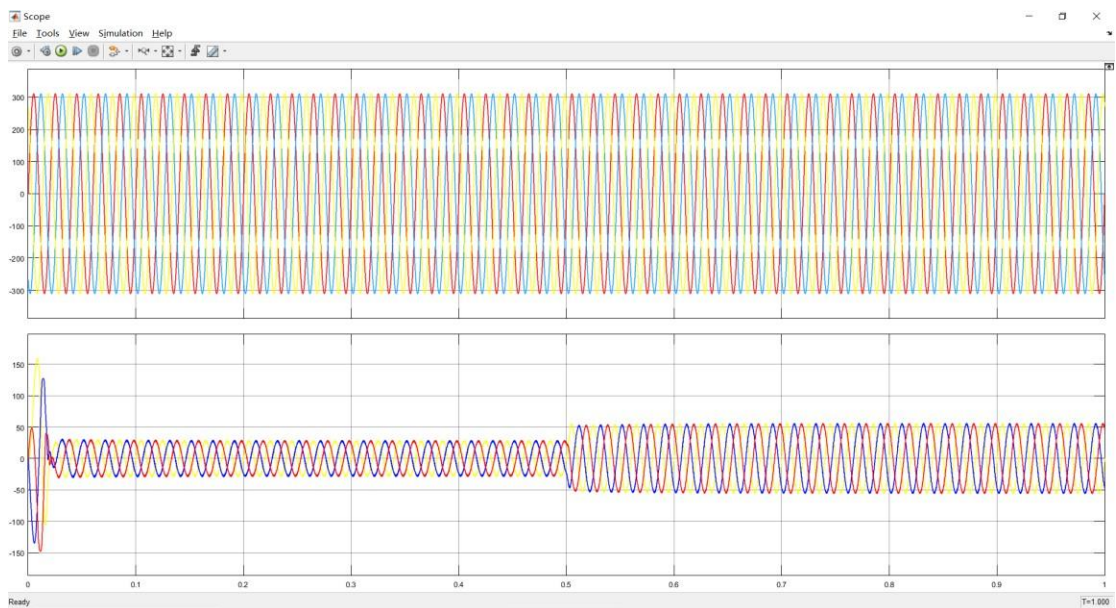


Figure 4.11 Waveform of three-phase voltage and current

To emphasize the benefits of high-frequency PWM, the simulation also tested the AC current waveform during low-frequency PWM, depicted in Figure 4.12 for analysis. It can be seen that the harmonics in the circuit are very high, up to 16.57%. At high frequencies, it is only 4.28%.

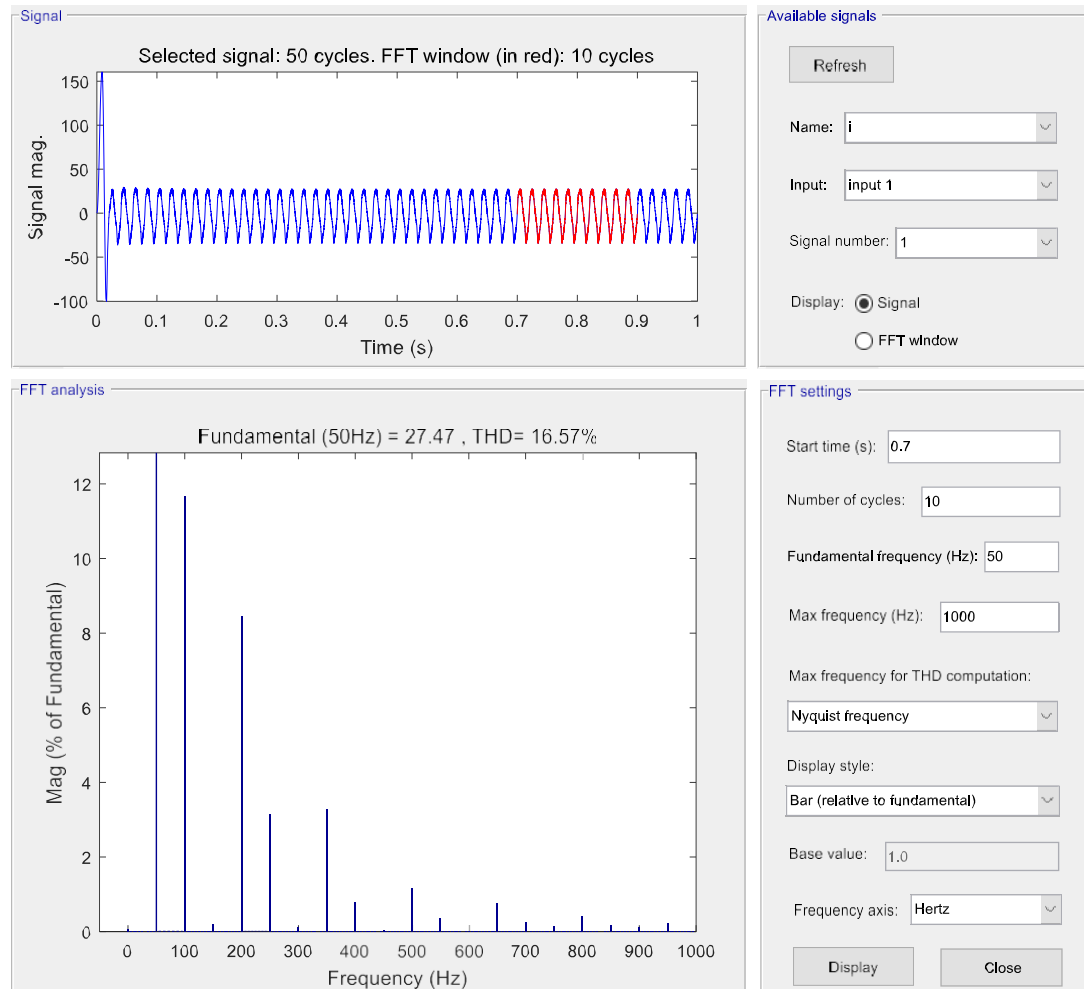


Figure 4.12 THD analysis diagram of A-phase current

Moreover, in real-world systems, the advantages of high-frequency PWM over low-frequency PWM mainly include the following points:

1. Reducing electromagnetic interference: High frequency PWM can reduce electromagnetic interference in circuits because at high frequencies, the switching speed of switching devices is faster, and the high-frequency noise generated can be more easily filtered out through filters, thereby improving the anti-interference ability of the entire system.

2. Reduction of inductance device size: Incorporating high-frequency PWM results in smoother current wave forms across inductive components, allowing for

downsizing of necessary inductance devices. This downsizing contributes to a reduction in the overall system's volume and weight.

3. Decrease the dimensions of the output filter: Utilizing high-frequency PWM results in a reduction in the size of the output filter. This is attributed to the enhanced efficacy of the output filter in eliminating high-frequency components within the PWM waveform at higher frequencies, thereby enabling the utilization of smaller filter components.

4. Improve system dynamic response: Increased PWM frequency enhances system dynamic response by leveraging the swifter switching speed of devices at higher frequencies. This enables faster responsiveness to control signals, thus enhancing overall system dynamics.

5. Reduce harmonic distortion: High frequency PWM can reduce harmonic distortion in the system because at high frequencies, smaller filter components are required, and the switching speed of switching devices is faster, which helps to reduce the impact of harmonic components.

To effectively demonstrate the benefits of three-phase PWM rectifiers, experiments were conducted on diode uncontrolled rectification circuits, illustrated in Figure 4.13. In this setup, the output voltage remains unregulated, and achieving a unit power factor for the grid-side voltage and current is unattainable, lacking adjustability. Figure 4.14 depicts the waveform of voltage and current in this configuration.

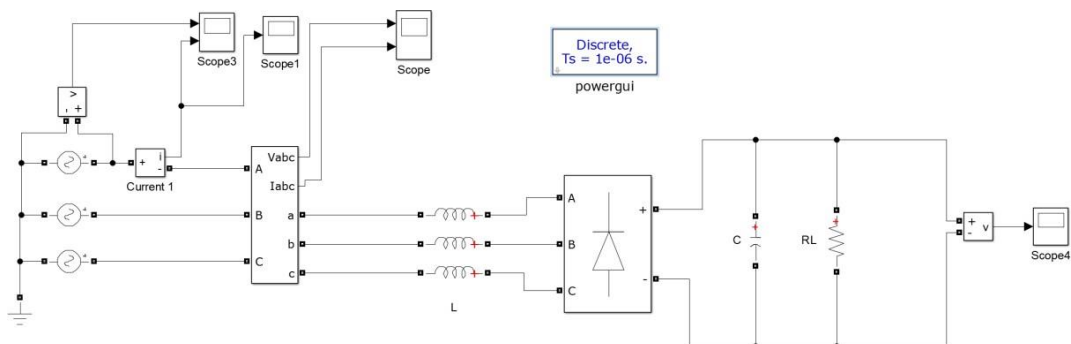


Figure 4.13 Simulated circuit diagram

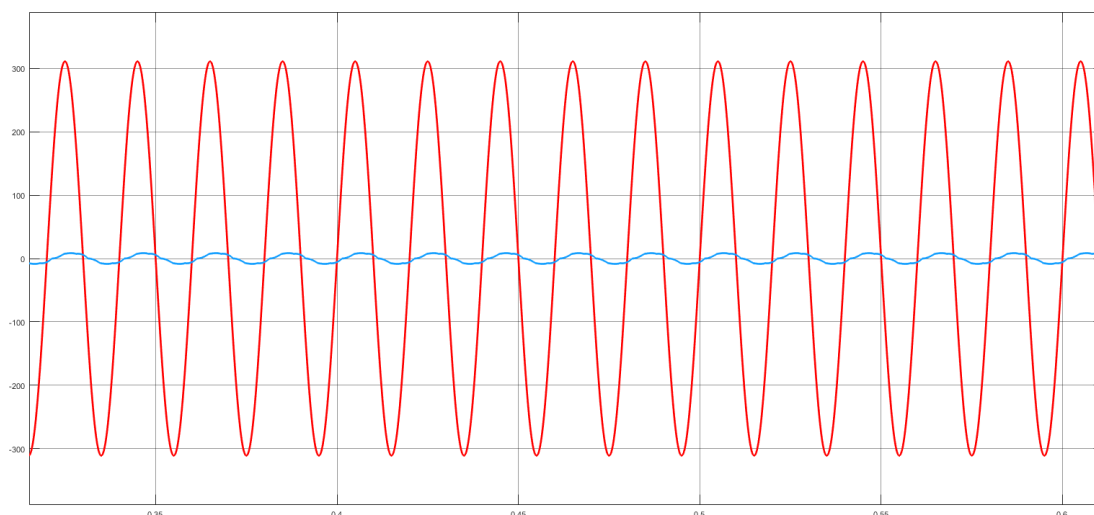


Figure 4.14 Voltage and current waveform diagram

Therefore, we can summarize the advantages of three-phase PWM rectifiers as follows:

1. **Efficient performance:** The three-phase PWM rectifier can achieve precise control of voltage and current by adjusting the PWM waveform, thereby improving rectification efficiency and reducing energy loss.

2. **Low harmonic distortion:** Through PWM control, three-phase PWM rectifiers can effectively reduce harmonic distortion of output voltage and current, making the output more stable and pure, and reducing interference with the power grid and other equipment.

3. **High reliability:** Due to the use of modern PWM control technology, three-phase PWM rectifiers have high reliability and stability, and can adapt to various working environments and load conditions.

4. **Small size and light weight:** Compared with traditional rectifiers, three-phase PWM rectifiers have smaller size and lighter weight under the same power output, making them suitable for applications with limited space or high requirements for lightweight.

5. **Strong flexibility:** By adjusting the frequency and duty cycle of the PWM signal, flexible adjustment of voltage and frequency can be achieved to meet different power conversion and control needs.

6. **Fast response speed:** The PWM control method of the three-phase PWM rectifier makes it fast in response, capable of quickly adjusting the output voltage and current, suitable for situations with high dynamic performance requirements.

4.4 Summary

This chapter mainly conducts Simulink simulation construction and waveform analysis on three-phase PWM rectifiers, and analyzes the system from two aspects: steady-state and dynamic.

CHAPTER 5

CONCLUSIONS AND RECOMMENDATIONS

5.1 Conclusions

A comprehensive and detailed analysis was conducted on the operational principles and performance characteristics of a three-phase voltage-type PWM rectifier. Mathematical models were established in three different coordinate systems. The conditions for the main circuit inductance and capacitance to meet the tracking characteristics were studied, and their respective range expressions were obtained; The design's validity was verified by examining the waveform diagrams of voltage outer loop control and current inner loop control, using a simulation model created on the Matlab platform for a three-phase voltage source PWM rectifier.

5.2 Recommendations for future work

In the next stage, we will continue to conduct in-depth research on three-phase rectifier circuits, analyze their different control strategies, and adopt more effective controls. Not only that, it is also necessary to learn about physical power electronics, rather than just staying in the computer simulation stage.

REFERENCES

- K. Hanna, 2007. "Adsorption of aromatic carboxylate compounds on the surface of synthesized iron oxide-coated sands," *Applied Geochemistry*, vol. 22, pp. 2045-2053, 2007.
- B. Zhang, J. Cohen, R. Ferrence, and J. Rehm, 2006. "The impact of tobacco tax cuts on smoking initiation among Canadian young adults," *American Journal of Preventive Medicine*, vol. 30, pp. 474-479, 2006.
- N. Geetha, S. Parvathy, and K. Sindhu Thampatty, 2017. "Output voltage regulation of controlled rectifiers using feedback linearization control algorithm," in *IEEE International Conference on Signal Processing, Informatics, Communication and Energy Systems*, Kollam, 2017, pp. 1-7.
- A. Hadri-Hamida, A. Allag, and S. M. Mimoune, 2008. "Adaptive nonlinear control of ac-dc PWM converter feeding induction heating," *Advances in Modelling and Analysis C*, vol. 1-2, no. 63, pp. 40-51, 2008.
- D. C. Lee, 2000. "Advanced nonlinear control of three-phase PWM rectifiers," *IEE Proceedings: Electric Power Applications*, vol. 147, no. 5, pp. 361-366, 2000.
- L. Huang, L. Yu, S. Quan, et al., 2017. "Design of voltage loop for three-phase PWM rectifier based on single neuron adaptive PID control," in *32nd Youth Academic Annual Conference of Chinese Association of Automation (YAC)*, Hefei, 2017, pp. 171-175.
- A. Fekik, H. Denoun, and N. Benamrouche, 2015. "A fuzzy-logic based controller for three phase PWM rectifier with voltage oriented control strategy," *International Journal of Circuits, Systems and Signal Processing*, vol. 9, pp. 412-419, 2015.
- Q. Yin, R. Lu, Q. Wang, et al., 2015. "Research on the neural network based adaptive PI controller of LCL-Filtered voltage source rectifier," *Journal of Computational and Theoretical Nanoscience*, vol. 7, no. 12, pp. 1317-1322, 2015.
- W. Qi, H. Wang, X. Tan, et al., 2014. "A novel active power decoupling single-phase PWM rectifier topology," in *IEEE Applied Power Electronics Conference and Exposition*, Fort Worth, 2014, pp. 89-95.
- M. Hao, L. Sun, Z. Yao, et al., 2014. "The Simulation of SVPWM Rectifier," in *International Symposium on Computer, Consumer and Control*, Taichung, Taiwan, 2014, pp. 642-645.
- M. H. Hedayati, A. B. Acharya, and V. John, 2013. "Common-Mode Filter Design for PWM Rectifier-Based Motor Drives," *IEEE Transactions on Power Electronics*, vol. 28, no. 11, pp. 5364-5371, 2013.

M. Hartmann, H. Ertl, and J. W. Kolar, 2011. "EMI Filter Design for a 1 MHz, 10 kW ThreePhase/Level PWM Rectifier," *IEEE Transactions on Power Electronics*, vol. 26, no. 4, pp. 1192-1204, 2011.

L. Gu and K. Jin, 2015. "A Three-Phase Isolated Bidirectional AC/DC Converter and its Modified SVPWM Algorithm," *IEEE Transactions on Power Electronics*, vol. 30, no. 10, pp. 5458-5468, 2015.

D. Lauria, 2014. "Design and control of an advanced PV inverter," *Solar Energy*, vol. 110, pp. 533-542, 2014.


M. Ben Said-Romdhane, M. W. Naouar, I. Slama-Belkhodja, et al., 2013. "Sliding Mode Direct Power Control of three-phase PWM boost rectifier using a single DC current sensor," in *IEEE Industrial Electronics Society*, 2013, pp. 1266-1271.

H. Yang, Y. Zhang, J. Liang, et al., 2018. "Sliding-Mode Observer Based Voltage-Sensorless Model Predictive Power Control of PWM Rectifier Under Unbalanced Grid Conditions," *IEEE Transactions on Industrial Electronics*, vol. 65, no. 7, pp. 5550, 2018.

APPENDICES

APPENDIX A: Graphs

The datasheet of IGBT:

Technische Information / Technical information		eupec			
IGBT-Module IGBT-modules		FZ3600R17KE3			
					
		Vorläufige Daten preliminary data			
IGBT-Wechselrichter / IGBT-inverter					
Höchstzulässige Werte / Maximum rated values					
Kollektor-Emitter-Sperrspannung collector-emitter voltage	$T_{vj} = 25^{\circ}\text{C}$	V_{CES}	1700	V	
Kollektor-Dauerleichstrom DC-collector current	$T_C = 80^{\circ}\text{C}$ $T_C = 25^{\circ}\text{C}$	$I_{c\ nom}$ I_c	3600 4800	A	A
Periodischer Kollektor Spitzenstrom repetitive peak collector current	$t_p = 1\ \text{ms}, T_C = 80^{\circ}\text{C}$	I_{CRM}	7200	A	
Gesamt-Verlustleistung total power dissipation	$T_C = 25^{\circ}\text{C}$	P_{tot}	18,0	kW	
Gate-Emitter-Spitzenspannung gate-emitter peak voltage		V_{GES}	+/-20	V	
Charakteristische Werte / Characteristic values					
			min.	typ.	max.
Kollektor-Emitter Sättigungsspannung collector-emitter saturation voltage	$I_c = 3600\ \text{A}, V_{GE} = 15\ \text{V}, T_{vj} = 25^{\circ}\text{C}$ $I_c = 3600\ \text{A}, V_{GE} = 15\ \text{V}, T_{vj} = 125^{\circ}\text{C}$	$V_{CE\ sat}$	2,00 2,40	2,45	V
Gate-Schwellenspannung gate threshold voltage	$I_c = 145\ \text{mA}, V_{CE} = V_{GE}, T_{vj} = 25^{\circ}\text{C}$	V_{GEth}	5,2	5,8	6,4
Gateladung gate charge	$V_{GE} = -15\ \text{V} \dots +15\ \text{V}$	Q_G	42,0		μC
Interner Gatewiderstand internal gate resistor	$T_{vj} = 25^{\circ}\text{C}$	R_{Gint}	0,5		Ω
Eingangskapazität input capacitance	$f = 1\ \text{MHz}, T_{vj} = 25^{\circ}\text{C}, V_{CE} = 25\ \text{V}, V_{GE} = 0$	C_{ies}	325		nF
Rückwirkungskapazität reverse transfer capacitance	$f = 1\ \text{MHz}, T_{vj} = 25^{\circ}\text{C}, V_{CE} = 25\ \text{V}, V_{GE} = 0$	C_{res}	10,5		nF
Kollektor-Emitter Reststrom collector-emitter cut-off current	$V_{CE} = 1700\ \text{V}, V_{GE} = 0\ \text{V}, T_{vj} = 25^{\circ}\text{C}$	I_{CES}		5,0	mA
Gate-Emitter Reststrom gate-emitter leakage current	$V_{CE} = 0\ \text{V}, V_{GE} = 20\ \text{V}, T_{vj} = 25^{\circ}\text{C}$	I_{GES}		400	nA
Einschaltverzögerungszeit (ind. Last) turn-on delay time (inductive load)	$I_c = 3600\ \text{A}, V_{CE} = 900\ \text{V}$ $V_{GE} = \pm 15\ \text{V}, R_{Gon} = 0,4\ \Omega, T_{vj} = 25^{\circ}\text{C}$ $V_{GE} = \pm 15\ \text{V}, R_{Gon} = 0,4\ \Omega, T_{vj} = 125^{\circ}\text{C}$	$t_{d\ on}$	0,73 0,78		μs μs
Anstiegszeit (induktive Last) rise time (inductive load)	$I_c = 3600\ \text{A}, V_{CE} = 900\ \text{V}$ $V_{GE} = \pm 15\ \text{V}, R_{Gon} = 0,4\ \Omega, T_{vj} = 25^{\circ}\text{C}$ $V_{GE} = \pm 15\ \text{V}, R_{Gon} = 0,4\ \Omega, T_{vj} = 125^{\circ}\text{C}$	t_r	0,21 0,23		μs μs
Abschaltverzögerungszeit (ind. Last)	$I_c = 3600\ \text{A}, V_{CE} = 900\ \text{V}$				
Gate-Emitter Reststrom gate-emitter leakage current	$V_{CE} = 0\ \text{V}, V_{GE} = 20\ \text{V}, T_{vj} = 25^{\circ}\text{C}$	I_{GES}		400	nA
Einschaltverzögerungszeit (ind. Last) turn-on delay time (inductive load)	$I_c = 3600\ \text{A}, V_{CE} = 900\ \text{V}$ $V_{GE} = \pm 15\ \text{V}, R_{Gon} = 0,4\ \Omega, T_{vj} = 25^{\circ}\text{C}$ $V_{GE} = \pm 15\ \text{V}, R_{Gon} = 0,4\ \Omega, T_{vj} = 125^{\circ}\text{C}$	$t_{d\ on}$	0,73 0,78		μs μs
Anstiegszeit (induktive Last) rise time (inductive load)	$I_c = 3600\ \text{A}, V_{CE} = 900\ \text{V}$ $V_{GE} = \pm 15\ \text{V}, R_{Gon} = 0,4\ \Omega, T_{vj} = 25^{\circ}\text{C}$ $V_{GE} = \pm 15\ \text{V}, R_{Gon} = 0,4\ \Omega, T_{vj} = 125^{\circ}\text{C}$	t_r	0,21 0,23		μs μs
Abschaltverzögerungszeit (ind. Last) turn-off delay time (inductive load)	$I_c = 3600\ \text{A}, V_{CE} = 900\ \text{V}$ $V_{GE} = \pm 15\ \text{V}, R_{Goff} = 0,5\ \Omega, T_{vj} = 25^{\circ}\text{C}$ $V_{GE} = \pm 15\ \text{V}, R_{Goff} = 0,5\ \Omega, T_{vj} = 125^{\circ}\text{C}$	$t_{d\ off}$	1,50 1,80		μs μs
Fallzeit (induktive Last) fall time (inductive load)	$I_c = 3600\ \text{A}, V_{CE} = 900\ \text{V}$ $V_{GE} = \pm 15\ \text{V}, R_{Goff} = 0,5\ \Omega, T_{vj} = 25^{\circ}\text{C}$ $V_{GE} = \pm 15\ \text{V}, R_{Goff} = 0,5\ \Omega, T_{vj} = 125^{\circ}\text{C}$	t_f	0,18 0,32		μs μs
Einschaltverlustenergie pro Puls turn-on energy loss per pulse	$I_c = 3600\ \text{A}, V_{CE} = 900\ \text{V}, L_S = 40\ \text{nH}$ $V_{GE} = \pm 15\ \text{V}, R_{Gon} = 0,4\ \Omega, T_{vj} = 25^{\circ}\text{C}$ $V_{GE} = \pm 15\ \text{V}, R_{Gon} = 0,4\ \Omega, T_{vj} = 125^{\circ}\text{C}$	E_{on}	495 745		mJ mJ
Abschaltverlustenergie pro Puls turn-off energy loss per pulse	$I_c = 3600\ \text{A}, V_{CE} = 900\ \text{V}, L_S = 40\ \text{nH}$ $V_{GE} = \pm 15\ \text{V}, R_{Goff} = 0,5\ \Omega, T_{vj} = 25^{\circ}\text{C}$ $V_{GE} = \pm 15\ \text{V}, R_{Goff} = 0,5\ \Omega, T_{vj} = 125^{\circ}\text{C}$	E_{off}	1050 1450		mJ mJ
Kurzschlussverhalten SC data	$t_p \leq 10\ \mu\text{s}, V_{GE} \leq 15\ \text{V}$ $T_{vj} \leq 125^{\circ}\text{C}, V_{CC} = 1000\ \text{V}, V_{CEmax} = V_{CES} - L_{VCE} \cdot di/dt$	I_{SC}	14000		A
Innere Wärmewiderstand thermal resistance, junction to case	pro IGBT per IGBT	R_{thJC}		7,00	K/kW
Übergangs-Wärmewiderstand thermal resistance, case to heatsink	pro IGBT / per IGBT $\lambda_{Paste} = 1\ \text{W/(m}\cdot\text{K)} / \lambda_{grease} = 1\ \text{W/(m}\cdot\text{K)}$	R_{thCH}	6,00		K/kW
prepared by: Martin Wölz	date of publication: 2003-4-11				
approved by: Christoph Lübke	revision: 2.0				

Technische Information / Technical information		eupec			
IGBT-Module IGBT-modules		FZ3600R17KE3			
					
Vorläufige Daten preliminary data					
Diode-Wechselrichter / Diode-inverter					
Höchstzulässige Werte / Maximum rated values					
Periodische Spitzenspannung repetitive peak reverse voltage	$T_{vj} = 25^{\circ}\text{C}$	V_{RRM}	1700	V	
Dauergleichstrom DC forward current		I_F	3600	A	
Periodischer Spitzenstrom repetitive peak forward current	$t_p = 1 \text{ ms}$	I_{FRM}	7200	A	
Grenzlastintegral I^2t - value	$V_R = 0 \text{ V}, t_p = 10 \text{ ms}, T_{vj} = 125^{\circ}\text{C}$	$\int I^2 dt$	1150	kA ² s	
Charakteristische Werte / Characteristic values					
Durchlassspannung forward voltage	$I_F = 3600 \text{ A}, V_{GE} = 0 \text{ V}, T_{vj} = 25^{\circ}\text{C}$ $I_F = 3600 \text{ A}, V_{GE} = 0 \text{ V}, T_{vj} = 125^{\circ}\text{C}$	V_F	min. 1,80 typ. 2,20 max. 2,20	V V V	
Rückstromspitze peak reverse recovery current	$I_F = 3600 \text{ A}, -di_F/dt = 14500 \text{ A}/\mu\text{s}$ $V_R = 900 \text{ V}, V_{GE} = -15 \text{ V}, T_{vj} = 25^{\circ}\text{C}$ $V_R = 900 \text{ V}, V_{GE} = -15 \text{ V}, T_{vj} = 125^{\circ}\text{C}$	I_{RM}	2800 3300	A A	
Sperrverzögerungsladung recovered charge	$I_F = 3600 \text{ A}, -di_F/dt = 14500 \text{ A}/\mu\text{s}$ $V_R = 900 \text{ V}, V_{GE} = -15 \text{ V}, T_{vj} = 25^{\circ}\text{C}$ $V_R = 900 \text{ V}, V_{GE} = -15 \text{ V}, T_{vj} = 125^{\circ}\text{C}$	Q_r	835 1450	μC μC	
Abschaltenergie pro Puls reverse recovery energy	$I_F = 3600 \text{ A}, -di_F/dt = 14500 \text{ A}/\mu\text{s}$ $V_R = 900 \text{ V}, V_{GE} = -15 \text{ V}, T_{vj} = 25^{\circ}\text{C}$ $V_R = 900 \text{ V}, V_{GE} = -15 \text{ V}, T_{vj} = 125^{\circ}\text{C}$	E_{rec}	590 1050	mJ mJ	
Innerer Wärmewiderstand thermal resistance, junction to case	pro Diode per diode	R_{thJC}		16,0	K/kW
Übergangs-Wärmewiderstand thermal resistance, case to heatsink	pro Diode / per diode $\lambda_{Paste} = 1 \text{ W}/(\text{m}\cdot\text{K})$ / $\lambda_{grease} = 1 \text{ W}/(\text{m}\cdot\text{K})$	R_{thCH}	13,0		K/kW

APPENDIX B: Tables

Simulation parameters

Parameter	Numerical value
AC voltage	220V, 50Hz
DC Voltage	800V
Input harmonic current	<5%
Power factor	>0.99
Power level	5kW
Network side inductance	20mH
DC capacitor	4mF